Using hilltop curvature to derive the spatial distribution of erosion rates

Martin D. Hurst,[1] Simon M. Mudd,[1] Rachel Walcott,[1] Mikael Attal,[1] and Kyungsoo Yoo[2]

Received 8 April 2011; revised 28 February 2012; accepted 1 March 2012; published 4 May 2012.

[1] Erosion rates dictate the morphology of landscapes, and therefore quantifying them is a critical part of many geomorphic studies. Methods to directly measure erosion rates are expensive and time consuming, whereas topographic analysis facilitates prediction of erosion rates rapidly and over large spatial extents. If hillslope sediment flux is nonlinearly dependent on slope then the curvature of hilltops will be linearly proportional to erosion rates. In this contribution we develop new techniques to extract hilltop networks and sample their adjacent hillslopes in order to test the utility of hilltop curvature for estimating erosion rates using high-resolution (1 m) digital elevation data. Published and new cosmogenic radionuclide analyses in the Feather River basin, California, suggest that erosion rates vary by over an order of magnitude (10 to 250 mm kyr^{-1}). Hilltop curvature increases with erosion rates, allowing calibration of the hillslope sediment transport coefficient, which controls the relationship between gradient and sediment flux. Having constraints on sediment transport efficiency allows estimation of erosion rates throughout the landscape by mapping the spatial distribution of hilltop curvature. Additionally, we show that hilltop curvature continues to increase with rising erosion rates after gradient-limited hillslopes have emerged. Hence hilltop curvature can potentially reflect higher erosion rates than can be predicted by hillslope gradient, providing soil production on hilltops can keep pace with erosion. Finally, hilltop curvature can be used to estimate erosion rates in landscapes undergoing a transient adjustment to changing boundary conditions if the response timescale of hillslopes is short relative to channels.

Citation: Hurst, M. D., S. M. Mudd, R. Walcott, M. Attal, and K. Yoo (2012), Using hilltop curvature to derive the spatial distribution of erosion rates, *J. Geophys. Res.*, *117*, F02017, doi:10.1029/2011JF002057.

1. Introduction

[2] The topographic form of landscapes reflects interplay between tectonics and climate-driven surface processes. These interactions dictate erosion rates and control topography since tectonic processes generally act to increase slope, while climate modifies the efficiency of erosional processes. Quantitative understanding of relationships between erosion rates and landscape morphology is essential to geomorphic and geochemical modeling efforts [e.g., *Tucker and Hancock*, 2010; *Yoo and Mudd*, 2008a]. Moreover, if critical relationships between topographic form and erosion rates can be identified, there is potential to interpret tectonic or climatic conditions based on topography alone [e.g., *Ahnert*, 1970; *Burbank et al.*, 1996; *Wobus et al.*, 2006a]. The interdependency of topography and erosion rate has been established through the demonstration that hillslope gradient and topographic relief increase with erosion rates [e.g., *Gilbert*, 1877; *Ahnert*, 1970; *Montgomery and Brandon*, 2002; *Palumbo et al.*, 2010]. However, several studies have identified that any such relationship breaks down at high erosion rates, as hillslope angles reach a limiting gradient [e.g., *Schmidt and Montgomery*, 1995; *Burbank et al.*, 1996; *Montgomery*, 2001; *Binnie et al.*, 2007; *Ouimet et al.*, 2009; *DiBiase et al.*, 2010; *Matsushi and Matsuzaki*, 2010].

[3] Characteristics of the longitudinal profiles of rivers have also been used successfully to infer the distribution of erosion rates in a landscape. Assuming channel form and evolution can be approximated by a model for bedrock channel evolution in which erosion rate is proportional to bed shear stress or stream power [*Whipple and Tucker*, 1999], the channel steepness index (a measure of channel slope normalized for drainage area) should increase with erosion rate [e.g., *Snyder et al.*, 2000; *Kirby et al.*, 2003; *Wobus et al.*, 2006a; *Kirby et al.*, 2007; *Ouimet et al.*, 2009; *Cyr et al.*, 2010; *DiBiase et al.*, 2010]. Both *Ouimet et al.* [2009] and *DiBiase et al.* [2010] demonstrated a nonlinear relationship between basin-averaged channel steepness indices and basin-averaged erosion rates in landscapes where hillslopes are invariantly steep. *Cyr et al.* [2010] demonstrated that channel steepness may reflect erosion

[1]School of Geosciences, University of Edinburgh, Edinburgh, UK.
[2]Department of Soil, Water, and Climate, University of Minnesota, St. Paul, Minnesota, USA.

0148-0227/12/2011JF002057

rates where hillslopes have become decoupled or lithological contrasts prevent hillslope gradient from being an appropriate topographic metric. Channel steepness indices have been particularly successful as an erosion rate metric in studies focusing at the scale of entire mountain belts, in landscapes with rapid erosion and steep hillslope gradients [e.g., *Ouimet et al.*, 2009; *DiBiase et al.*, 2010; *Kirby and Ouimet*, 2011].

[4] The relationship between fluvial incision rates and channel steepness indices is complicated by the existence of thresholds for fluvial erosion [*Snyder et al.*, 2003a, 2003b; *Attal et al.*, 2011] which have been demonstrated to cause nonlinearity in the relationship between channel steepness indices and erosion rate [*DiBiase and Whipple*, 2011]. Channel width adjustments in response to changes in boundary conditions [e.g., *Finnegan et al.*, 2005; *Whittaker et al.*, 2007a] may also influence the distribution of erosion and therefore steepness indices [e.g., *Attal et al.*, 2011], so quantifying variation in channel widths is important if one is to apply this erosion metric [e.g., *DiBiase and Whipple*, 2011; *Kirby and Ouimet*, 2011]. The presence/absence of fluvial sediment can also modulate erosion rates significantly [*Cowie et al.*, 2008].

[5] Channel steepness is an appropriate metric for erosion rate where valley forming process become dominantly fluvial (typically at drainage areas >1 km^2 [*J. D. Stock et al.*, 2005]). Such coarse resolution limits application at the hillslope scale, which is of interest if one is to understand sediment production and nutrient cycling [e.g., *Heimsath et al.*, 1997; *Yoo and Mudd*, 2008b; *Porder et al.*, 2007], and the processes that supply sediment to channels [e.g., *Roering et al.*, 2007, 2010]. The geomorphic characteristics of hillslopes have the potential to overcome this scale problem [*Mudd and Furbish*, 2007] and would not be subject to the same limitations as channel-based erosion rate metrics. Indeed, *DiBiase et al.* [2012] have recently shown that mean slope derived from high-resolution topography, and the amount of bare rock exposed on hillslopes scale with catchment averaged erosion rates.

[6] Our principal objective was to develop a method for using topographic metrics to infer erosion rates that (1) can be applied where erosion rates are rapid enough that hillslope gradients become invariably steep, (2) can be applied at hillslope or zero-order basin scale, and (3) can be applied in landscapes experiencing a range of erosion rates due to transient adjustment in the channel network. Our strategy used a novel technique which exploits the topography of hilltops throughout a landscape. It has previously been established that where hillslope sediment transport can be approximated as a nonlinear function of slope, the curvature of hilltops is linearly related to erosion rates [*Andrews and Bucknam*, 1987; *Roering et al.*, 1999]. Our approach relied on hilltops being soil mantled and assumptions that sediment transport on hilltops is dominated by creep-like processes, the efficacy of which is assumed spatially and temporally constant. Hilltop curvature has previously been used to predict erosion rates for individual hillslopes in landscapes where hilltops are soil mantled and assumed to be in steady state [*Roering et al.*, 2007, 2010]. Such an approach has not hitherto been applied across entire landscapes, or under conditions of landscape transience.

[7] In this contribution, we used a high-resolution (1 m) digital elevation model (DEM) derived by airborne light detection and ranging (lidar) by the National Center for Airborne Laser Mapping (NCALM). We used the DEM to compare hilltop curvature with erosion rates derived from cosmogenic radionuclides (CRN) in the Feather River basin in the northern Sierra Nevada of California. From the resulting relationship between erosion rate and hilltop curvature we estimated the efficiency of sediment transport, allowing us to predict erosion rates across the entire landscape. To do this, we developed new techniques to define hilltops and their adjacent dispersing hillslopes, and then extract the important geomorphic parameters of hilltop curvature, mean slope, hillslope relief and hillslope length.

2. Theoretical Background

[8] The form and evolution of hillslopes in soil-mantled landscapes has been predominantly investigated through principles of conservation of mass [*Dietrich et al.*, 2003]. Such an approach was first described qualitatively by *Gilbert* [1909] and expressed mathematically by *Culling* [1960]. Here we consider a hillslope in a moving reference frame where the surface elevation ζ [L], (dimensions of [M]ass, [L]ength and [T]ime denoted in square brackets) is measured relative to the elevation of a moving reference point ζ_0 [L] [see, e.g., *Mudd and Furbish*, 2005]. The surface elevation is then

$$\frac{\partial \zeta}{\partial t} = -\frac{\partial \zeta_0}{\partial t} - \nabla \cdot q_s, \tag{1}$$

where q_s [L^{2}T^{-1}] is volumetric sediment flux per unit width and t is time. We assume mass gain/loss because of aeolian processes is negligible. Our mass balance does not account for volume changes in soils due to chemical denudation. *Riebe et al.* [2001a] demonstrated that chemical denudation scales with total denudation in our study area, but that chemical denudation is small compared to physical denudation and should have minimal impact on hillslope morphology [e.g., *Mudd and Furbish*, 2004].

[9] The choice of reference is arbitrary but it is convenient to equate the lowering of the reference elevation to the rate of local bedrock lowering at the base of the hillslope (E, [L T^{-1}], i.e., the bedrock stream incision) such that $\partial\zeta_0/\partial$t = $-(\rho_r/\rho_s)E$ where ρ_r and ρ_s [ML^{-3}] are the densities of bedrock and dry soil, respectively. If the entire hillslope lowers at the same rate as the channel then equation (1) reduces to

$$\frac{\rho_r}{\rho_s} E = \nabla q_s. \tag{2}$$

On gently inclined hillslopes where gravity driven sediment flux occurs because of creep-like processes, q_s can be approximated as a linear function of slope. The convex profile of hillslopes was first attributed to slope-dependent soil creep by *Davis* [1892] and *Gilbert* [1909], who observed that hillslope gradients tended to increase steadily with distance from topographic divides (hilltops). Hillslopes often become planar away from topographic divides in high-relief landscapes, driven both by a process transition to landslide dominated sediment flux [e.g., *Roering et al.*, 1999; *Binnie et al.*, 2007] and the associated increase in particle displacement distances during transport [e.g., *Tucker and Bradley*, 2010; *Foufoula-Georgiou et al.*, 2010]. This

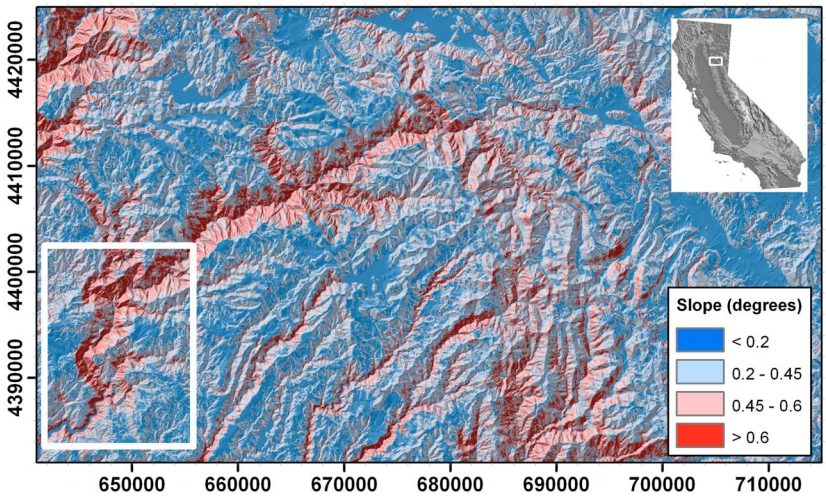

Figure 1. Shaded slope map for our study site in the Feather River (Middle Fork) basin, Sierra Nevada (inset map shows location of the study area in California). White box shows the extent of the Airborne Laser Swath Mapping (ALSM) derived topographic data set. The relict upland landscape with low slopes depicted in blue is dissected by the canyon of the Feather River and its tributaries with steeper slopes, depicted in red. The spatial reference system is Universal Transverse Mercator (UTM) Zone 10N with spatial units in meters.

transition can be approximated by coupling a linear, slope-dependent model for sediment flux driven by soil creep [e.g., *Culling*, 1960] with a threshold hillslope angle (S_{Th}) beyond which sediment flux is infinite so that steeper slopes cannot be maintained [e.g., *Howard*, 1994; *Densmore et al.*, 1998]:

$$q_s = -D\nabla\zeta; \quad \nabla\zeta < S_{Th} \tag{3a}$$

$$q_s = \infty; \quad \nabla\zeta \geq S_{Th}, \tag{3b}$$

where D [L^2T^{-1}] is a transport coefficient and ζ [L] is the elevation of the surface. A similar flux law was formulated allowing sediment flux to increase in a nonlinear fashion with hillslope gradient so that as slope approaches a critical angle (S_C), sediment flux asymptotically approaches infinity [*Andrews and Bucknam*, 1987; *Roering et al.*, 1999]:

$$q_s = -D\nabla\zeta\left[1 - \left(\frac{|\nabla\zeta|}{S_C}\right)^2\right]^{-1}. \tag{4}$$

When hillslope gradient, $\nabla\zeta$, is small enough for the bracketed term in equation (4) to be negligible, we can substitute equation (4) into equation (2) and solve for erosion rates where slope angles are low (i.e., on hilltops):

$$E = -\frac{\rho_s}{\rho_r} DC_{HT}, \tag{5}$$

where C_{HT} is the hilltop curvature, i.e., $\nabla^2\zeta$ at the hilltop, since this is where we expect slope to be lowest. Equation (5) states that the erosion rate on a steadily denuding hillslope is a linear function of the Laplacian of elevation at the hilltop C_{HT} and the transport coefficient. *Roering et al.* [2007] provided a comprehensive framework for analyzing relationships between denudation and topography. They nondimensionalized erosion rate and relief to allow comparisons between landscapes with distinct process rates and morphology and cast dimensionless erosion rate and relief as functions of readily quantifiable topographic parameters. Finally, *Roering et al.* [2007] defined dimensionless relief, R^* where relief was normalized according to $R^* = R/(S_c L_H)$ (hillslope relief R is the elevation difference between hilltop and channel ζ ($x = 0$) $-$ ζ ($x = L_H$)) and dimensionless erosion rate, $E^* = E/E_R$ where E_R [LT^{-1}] is a reference erosion rate defined by

$$E_R = \frac{DS_C}{2L_H(\rho_r/\rho_s)}. \tag{6}$$

Hence they arrived at the following definitions for dimensionless erosion rate E^* and relief R^*:

$$E^* = \frac{E}{E_R} = \frac{\rho_r}{\rho_s} \cdot \frac{2EL_H}{DS_C} = \frac{2C_{HT}L_H}{S_C} \tag{7a}$$

$$R^* = \frac{\overline{S}}{S_C} = \frac{1}{E^*}\left\{\sqrt{1+(E^*)^2} - \ln\left[\frac{1}{2}\left(1+\sqrt{1+(E^*)^2}\ \right)\right] - 1\right\}, \tag{7b}$$

where $\bar{S}$ is the mean gradient of the hillslope.

[10] Similar relationships can be derived for the threshold model (equation (3)) as described by *DiBiase et al.* [2010]:

$$R^* = 1 - \frac{1}{E^*}; \quad E^* \geq 2 \tag{8a}$$

$$R^* = \frac{E^*}{4}; \quad E^* < 2. \tag{8b}$$

Topographic parameters C_{HT}, L_H and $\bar{S}$ can be extracted from high-resolution topography, allowing relationships

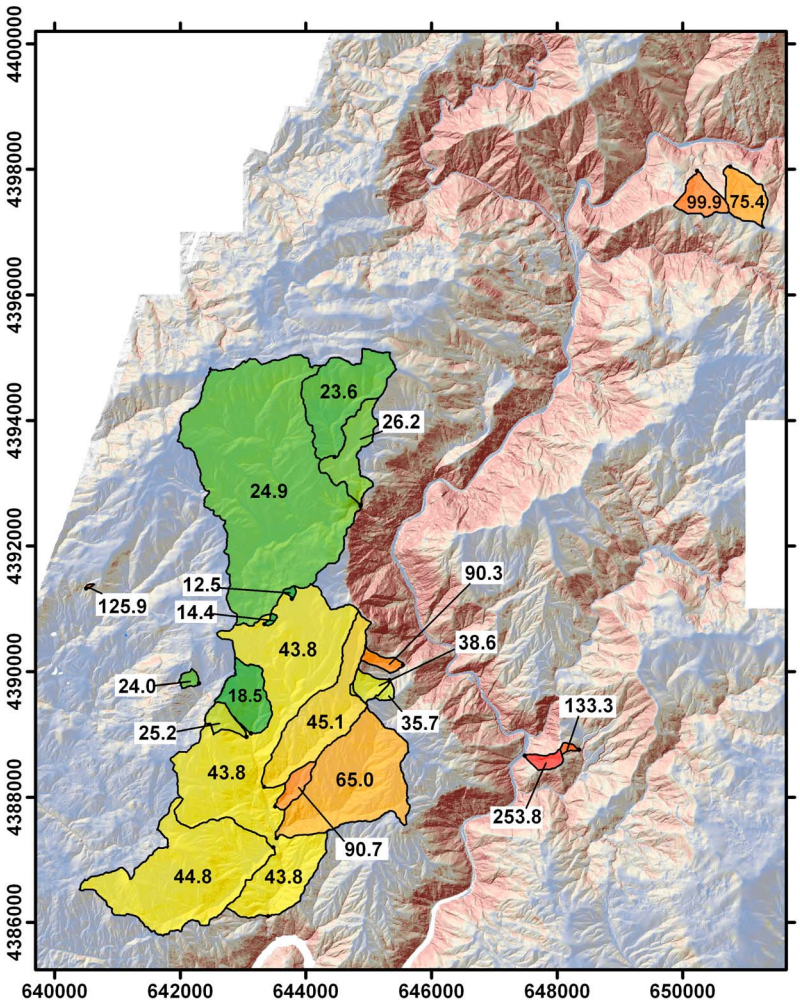

Figure 2. High-resolution (ALSM-derived) shaded slope map of study site (low gradients are blue, steep slopes are red). Overlain are cosmogenic radionuclides (CRN) sample sites with estimated basin-averaged erosion rates in mm kyr^{-1} (shaded green to red with increasing erosion rate). Samples were taken for basins exclusively in granitoid bedrock. Erosion rates vary over an order of magnitude from the canyon to the adjacent relict upland. The spatial reference system is UTM Zone 10N with spatial units in meters.

between erosion rate and topographic form to be investigated in a nondimensional framework. As erosion rate increases, relief initially increases, but since relief is limited (through S_{Th} or S_C), it becomes insensitive to changes at high erosion rates. The nonlinear and threshold models (equations (7) and (8), respectively) are distinct at intermediate erosion rates (E^* in range 1 to 10) where equation (7b) predicts lower R^* than equation (8b) for a given value of E^*. Therefore quantifying E^* and R^* may allow for distinguishing the applicability of flux models based on topography alone [*DiBiase et al.*, 2010].

[11] Both the threshold (equation (3)) and nonlinear (equation (4)) flux models have empirical and experiment support [e.g., *Gabet*, 2000; *Roering et al.*, 2001a; *Pelletier and Cline*, 2007]. Equation (5) is applicable in both cases since it could also be derived by substituting equation (3) (instead of (4)) into equation (2). Hilltop curvature should thus scale with erosion rates beyond the critical erosion rate for producing steep, planar hillslopes, providing soil production rates (SPR) on the hilltops can keep pace. The maximum attainable rate of soil production is critical to the application of hilltop curvature as a metric for erosion rate, since the ability of SPR on ridges to keep pace with erosion rates in adjacent channels is a prerequisite to the validity of equation (5). *Heimsath et al.* [2012] demonstrated that maximum soil production rates may themselves scale with erosion rates. Since equations (3) and (4) allow soil transport to tend to infinity on steep slopes, soil may be stripped and bedrock may be exposed on hillslopes. Despite this, we require hillslope material to remain readily transportable such that hilltop morphology is controlled by the ability to transport material rather than the ability to generate material from underlying bedrock.

[12] Critically the application of equation (5) to predict erosion rates does not require an entire drainage basin to be in steady state, but only that the hillslope adjacent to the channel should be fully adjusted to the rate of stream downcutting (i.e., uniform down wasting and a hilltop curvature adjusted to this lowering rate). Therefore, in a landscape where the response time of the hillslopes is short relative to that of the stream network, hillslope morphology

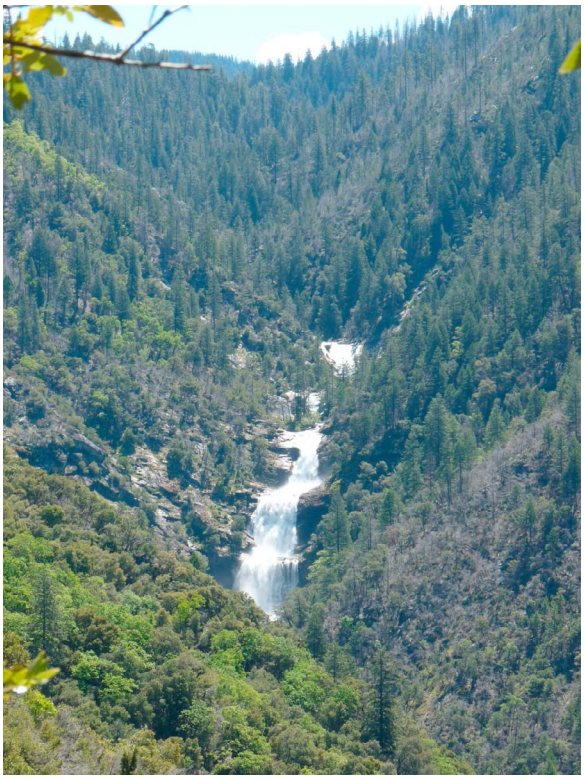

Figure 3. Photograph of Cascade River, a large tributary to Feather River. Channel is very steep because of passing of a knickpoint associated with increased erosion rate in the channel. Hillslopes remain soil mantled despite increased erosion rate.

should keep pace with channel erosion rates, permitting the use of hilltop curvature as a surrogate for erosion rate. The landscape of the northern Sierra Nevada, California, is undergoing a transient response (relative baselevel fall) to tectonic perturbation (see section 3) which allowed us to test the predictive power of hilltop curvature in a landscape containing a range of erosion rates.

3. Field Setting

[13] Our field site is located in the lower reaches of the Middle Fork Feather River, in the northern Sierra Nevada of California (Figure 1). Our study was focused in areas of Mesozoic granitoid plutons which were intruded into the Central belt terrain, consisting of late Triassic-Jurassic ophiolitic, volcanic and sedimentary units of the Fiddle Creek Complex [*Day and Bickford*, 2004]. The Sierra Nevada is a west-tilted fault block bound to the west by the San Andreas Fault system and to the east by the escarpment of a transtensional (dextral) frontal fault system [*Unruh*, 1991]. The westward tilting of the fault block is recorded in the topography by the tilting of a relict landscape with the western side of the range sloping gently away from the summit crest line to the Central Valley [*Saleeby et al.*, 2009]. The relict surface is dissected by main river drainages which have incised deep canyons (Figure 1).

[14] The relict surface has been interpreted as the remnant of the western edge of an orogenic plateau surface (Nevadoplano) which existed into the early Cenozoic [*Busby and Putirka*, 2009]. Apatite fission track (AFT) dates reveal an average erosion rate of 40 mm kyr^{-1} for the relict landscape, persisting until at least 32 million years ago (Ma) [*Cecil et al.*, 2006]. This is slightly higher than CRN-derived denudation rates (millennial timescale) reported for summit flats (2–19 mm kyr^{-1}) [*Small et al.*, 1997; *Riebe et al.*, 2000] and for low-relief basins on the relict surface (∼20–40 mm kyr^{-1}) [*Riebe et al.*, 2000; *G. M. Stock et al.*, 2005] in the study area. The Feather River traverses the northern Sierra Nevada, dissecting the relict surface to generate a deep canyon. This morphology is clear from the distribution of slope angles in the basin, with steep slopes (>∼0.6) mainly occurring immediately adjacent to the Feather River and the largest tributaries (Figure 1). The landscape transience was initiated by accelerated uplift circa 3.5–5 Ma [*Wakabayashi and Sawyer*, 2001; *Stock et al.*, 2004; *Clark et al.*, 2005], possibly caused by the delamination of an eclogite root beneath the mountain range [*Saleeby and Foster*, 2004; *Jones et al.*, 2004]. Alternatively isostatic unloading has been suggested as a possible uplift mechanism [*Small and Anderson*, 1995]. However, *G. M. Stock et al.* [2005] inferred that such a means is unable to account for all uplift in the Sierra Nevada and suggested delamination 10–3 Ma may have generated significant uplift. The associated onset of tilting and frontal faulting of the Sierra Nevada block likely resulted in the initiation of rapid fluvial incision [*Wakabayashi and Sawyer*, 2001]. Erosion rates in and adjacent to the canyon significantly exceed those predicted by AFT (>200 mm ka^{-1}) [*Riebe et al.*, 2000; *Wakabayashi and Sawyer*, 2001] (Figure 2). Long-term exhumation rates derived from (U-Th)/He ages fail to record late Cenozoic acceleration in denudation, implying that less than 3 km of the crust has been exhumed since the acceleration [*Cecil et al.*, 2006].

[15] Despite rapid denudation rates, much of the landscape remains forested and soil mantled (Figure 3). The modern climate is semiarid with a strong precipitation gradient from the dry Central Valley of California to the high elevations of the Sierra Nevada Mountains. Mean annual temperature (MAT) is 12.5°C and mean annual precipitation (MAP) is 1750 mm (data from the PRISM Climate Group, Oregon State University, http://prism.oregonstate.edu (accessed 7 July 2011) [*Daly et al.*, 1997]). The area remained largely unglaciated during the Pleistocene, except for its uppermost reaches [*Warhaftig and Birman*, 1965; *Clark*, 1995]. Erosion rates from low-relief areas in the Sierra Nevada are insensitive to spatial variation in climate [*Riebe et al.*, 2001b].

4. Methods

4.1. Denudation Rates From Cosmogenic Radionuclides

[16] Measuring the concentration of ^{10}Be in quartz from fluvial sediments in transport allows calculation of the basin averaged denudation rate [e.g., *Brown et al.*, 1995; *Granger et al.*, 1996; *Bierman and Steig*, 1996]. Here we report denudation rates using ^{10}Be concentrations reported by *Riebe et al.* [2000], plus 13 additional samples for catchments proximal to the Feather River (Figure 2).

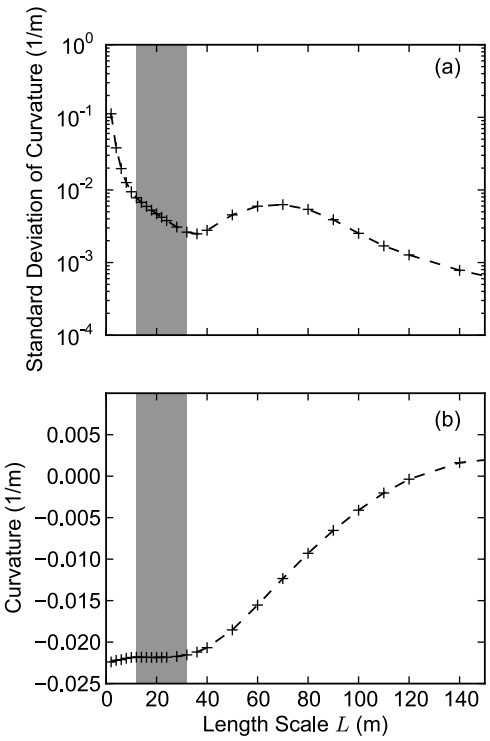

Figure 4. Influence of window size when calculating topographic curvature from gridded elevation data of a soil-mantled hillslope. (a) Standard deviation and (b) mean value of curvature for a sample hilltop known to be eroding at $\sim$36 $\pm$ 5 mm kyr^{-1}. A scaling break occurs at L = 12 m separating the signal of pit mound topography from that of hillslope morphology. Curvature values are consistent up to L = 32 m at which point adjacent valley bottoms start to influence curvature.

[17] For the additional samples, quartz separation and ^{10}Be isolation was carried out at the University of Edinburgh's Terrestrial Cosmogenic Nuclide Laboratory following standard techniques [see *Bierman et al.*, 2002], with accelerator mass spectrometry (AMS) performed at PrimeLab (Purdue University) to measure the concentration of ^{10}Be in the samples. We interpret these concentrations in terms of an erosion rate using the Cosmic-Ray Produced Nuclide Systematics on Earth Project online calculator version 2.2 (http://hess.ess.washington.edu/, accessed September 2010) to determine basin-wide erosion rates [*Balco et al.*, 2008]. While this tool is designed to calculate site specific denudation rates, it can also be used to calculate basin-wide denudation rates by using a production-weighted mean elevation and mean shielding factor for the catchment area. We calculate topographic shielding according to *Codilean* [2006] and scale production according to a basin averaged shielding factor.

[18] Cosmic radiation can also be shielded from the surface through snow cover. Snow fall data from 2002 to 2009 from the nearest and lowest observation station (Four Trees; elevation 1600 m) indicates that snow water equivalent depths averaging 74 cm cover the ground for five months of the year [*National Operational Hydrologic Remote Sensing Center*, 2004]. Following *Gosse and Phillips* [2001] this equates to a snow shielding factor of 0.73. While such significant snowfall may shield the surface from incoming cosmic radiation, we note that the observation station is >600 m higher than the maximum elevations at our field site and thus expect snow shielding to be significantly less for our samples. Here we do not account for snow shielding, but recognize that we may be overestimating erosion rates as a result, most significantly for the slowest eroding portions of the landscape, since these sample sites are highest in elevation (900–1000 m).

4.2. Topographic Slope and Curvature

[19] Here topographic curvature is defined as the two dimensional Laplacian ($C = \nabla^2\zeta$) of the function defining the surface $\zeta = f(x, y)$ [*Moore et al.*, 1991]. Both 6 term quadratic and 9 term polynomial functions have been routinely fitted to elevation data to approximate the land surface [e.g., *Evans*, 1980; *Zevenbergen and Thorne*, 1987; *Moore et al.*, 1991]. *Schmidt et al.* [2003] compared methods for 10 m resolution gridded data, using both an analytical and real landscape. They concluded that fitting 9 term polynomials was appropriate where elevation data are reliable; however, quadratics were better fitted where the data set quality is poor. We carried out a similar comparison for high-resolution (lidar) topography for both gridded and ungridded data and found that the results were indistinguishable. Consequently, we favored fitting a 6 term function, working with gridded elevations to minimize computation time. An algorithm was created to fit a surface by least squares regression to a local window of elevations. The fitted surface has the form

$$\zeta = ax^2 + by^2 + cxy + dx + ey + f, \tag{9a}$$

with curvature (C) and slope (S) calculated from the fitted coefficients [*Evans*, 1980] according to

$$C = 2a + 2b \tag{9b}$$

$$S = \sqrt{d^2 + e^2}. \tag{9c}$$

The length scale L dictates the size of the moving window of elevations to which equation (9a) is fitted. We perform the regression on the gridded data using an unweighted, square window of size $L \times L$ in which the cell of interest is at the center. Since this method does not require the fitted surface to pass through any DEM nodes, it is acting to smooth the surface and so no preprocessing to smooth the lidar data was performed. We tested this approach against performing regression on the bare earth point cloud data [e.g., *Roering et al.*, 2010] and found the results indistinguishable.

[20] In forested landscapes, lidar-derived digital topography commonly exhibits strong local variability because of the presence of pits associated with the upheaval or decay of tree root clumps [e.g., *Roering et al.*, 2010], or dense vegetation which has been treated as bare earth [*Lashermes et al.*, 2007]. Thus standard algorithms computing slope and curvature from 3 $\times$ 3 pixel moving windows produce noisy results. To investigate variation in topographic metrics at the scale of entire hillslopes requires quantifying them over a greater spatial extent. The length scale over which these metrics should be calculated is determined by a break in

Table 1. Cosmogenic Radionuclides Sample Information and Calculated Denudation Rates

Sample	Location (Decimal °N/°W)	Weighted Mean Elevation[a] (m)	Shielding Factor[b]	Quartz Weight[c] (g)	Be Carrier Weight (mg)	$^{10}Be/^{9}Be$[d,e,f] ($\times 10^{-15}$)	^{10}Be Concentration[e,f,g] (10^5 atoms g^{-1} SiO_2)	Denudation Rate[h,i] (kyr^{-1})
FR-2	39.6604/121.3607	909.0	0.995	n/a	n/a	48 ± 8	0.52 ± 0.08	125.9 ± 23.2
FR-4	39.6359/121.2783	496.5	0.985	n/a	n/a	36 ± 9	0.20 ± 0.05	253.8 ± 66.6
FR-5	39.6361/121.2714	571.0	0.994	n/a	n/a	33 ± 7	0.40 ± 0.09	133.3 ± 31.9
FR-6	39.6385/121.3322	917.4	0.998	n/a	n/a	279 ± 12	2.56 ± 0.16	25.2 ± 2.7
FR-7	39.6391/121.3311	907.0	0.992	n/a	n/a	341 ± 13	3.41 ± 0.22	18.5 ± 2.0
FR-8	39.6586/121.3230	1055.7	1	n/a	n/a	556 ± 15	5.52 ± 0.31	12.5 ± 1.4
FR-9	39.6552/121.3269	1032.5	1	n/a	n/a	473 ± 19	4.76 ± 0.31	14.4 ± 1.6
FR-10	39.6465/121.3434	966.5	1	n/a	n/a	203 ± 9	2.75 ± 0.19	24.3 ± 2.7
BRB-2	39.6491/121.3020	841.1	1	56.89	248	576 ± 32	1.57 ± 0.09	38.6 ± 3.4
BRB-6	39.6463/121.3061	800.5	1	54.45	249	633 ± 22	1.76 ± 0.18	35.7 ± 4.7
BRB-8	39.6483/121.3036	808.7	1	54.43	248	268 ± 13	0.71 ± 0.04	90.3 ± 8.5
BEAN-1	39.6126/121.3295	782.2	0.997	47.84	249	422 ± 10	1.42 ± 0.04	43.8 ± 3.7
BEAN-2	39.6225/121.3283	695.5	0.997	49.24	245	401 ± 9	1.31 ± 0.04	44.8 ± 3.7
BEAN-4	39.6237/121.3273	717.9	0.997	54.47	243	314 ± 8	0.92 ± 0.03	65.0 ± 5.3
BEAN-5	39.6312/121.3298	825.9	0.998	41.02	255	347 ± 8	1.42 ± 0.04	45.1 ± 3.8
BEAN-7	39.6284/121.3277	671.7	0.995	45.70	246	184 ± 5	0.64 ± 0.02	90.7 ± 7.2
FT-3	39.6714/121.3109	1065.9	1	19.82	249	858 ± 22	2.85 ± 0.09	26.2 ± 2.3
FT-4	39.6712/121.3109	1007.6	1	52.17	249	906 ± 24	2.88 ± 0.09	24.9 ± 2.2
FT-6	39.6784/121.3155	1097.0	1	50.86	249	994 ± 15	3.23 ± 0.10	23.6 ± 2.1
BS-1	39.7184/121.2473	966.4	0.993	56.75	250	244 ± 14	0.70 ± 0.04	99.9 ± 9.7
SB-1	39.7189/121.2411	1015.0	0.991	59.71	250	350 ± 15	0.96 ± 0.04	75.4 ± 6.6

[a]Mean elevation weighted by spallogenic production in each digital elevation model pixel in the basin (calculated following *Stone* [2000]).
[b]Calculated according to *Codilean* [2006].
[c]A density of 2.6g/cm^3 was assumed.
[d]Isotope ratios were normalized to ^{10}Be standards prepared by *Nishiizumi et al.* [2007] $^{10}Be/^{9}Be$ ratio of 2.85 ± 10^{-12} (KNSTD07).
[e]Isotope ratios for FR-2 to FR-10 were normalized to National Institute of Standards and Technology standard material (NIST certified) with $^{10}Be/^{9}Be$ ratio of 2.68 ± 10^{-11} [*Riebe et al.*, 2000]. These data are scaled to the KNSTD07 standard using a factor of 1.0425 [*Balco et al.*, 2008].
[f]Uncertainties are reported at 1σ confidence.
[g]A blank value of $^{10}Be/^{9}Be = 35.63 \pm 10^{-15}$ was used to correct for background.
[h]Production rates were scaled according to *Dunai* [2000].
[i]Beryllium-10 erosion rates were calculated with the Cosmic-Ray Produced Nuclide Systematics on Earth Project online calculator [*Balco et al.*, 2008] version 2.2 (http://hess.ess.washington.edu/). Propagated error accounts for uncertainty in $^{10}Be/^{9}Be$ ratio measurement and production scaling only.

indicators of variability as a function of length scale. *Lashermes et al.* [2007] demonstrated that a length scale L of 12 m was appropriate in the South Fork Eel River, while *Roering et al.* [2010] demonstrated $L = 15$ m in their forested landscape in the Oregon Coastal Range (using a search radius of 7.5 m, hence $L = 2 \times$ window radius). Figure 4 shows the standard deviation of curvature as a function of length scale for a portion of steadily denuding hilltop in a tributary to the Feather River basin ($E \sim 36$ +/− 5 mm kyr^{-1}; sample BRB-6; see Table 1). A scaling break exists at $L = 12$ m, which dictates the length scale over which we report curvature for the entire landscape.

4.3. Mapping Hilltops

[21] Hilltops were delineated from topographic data as the intersecting margins of basins at all stream orders (zero order and upward) using ARC GIS software and scripting with Python. The stream network was defined to allow extraction of drainage basins at a range of stream orders whose adjoining margins were defined as hilltops.

[22] Identification of trails and roads was crudely automated by filtering the DEM for pixels with positive curvature and low slope which have extreme values of both positive and negative curvature within a 10 m radius. The resulting areas were preferentially smoothed to aid extraction of the stream network, and excluded from later hillslope analysis. To define the extent of the valley network we implemented the Geonet tool (in MATLAB) made publicly available by *Passalacqua et al.* [2010]. This tool identifies the likely location of channel heads based on a curvature threshold following nonlinear smoothing of the DEM. This filtering smoothes low-relief, high-frequency noise yet preserves sharp features such as hillslope-to-valley transitions. Once likely channel heads were identified a steepest descent trace was run from each to create a vector network of the valley system. Thus we ensured sampling of zero-order basins, regardless of the dominant valley-forming process. Strahler stream order [*Strahler*, 1952] was calculated from the resulting valley bottom network, and drainage basins mapped for the downstream termination of each stream segment with a given stream order. A vector network of intersecting basin margins was generated and filtered to exclude slopes of >0.4 (beyond which sediment transport typically has a >15% nonlinear component) since we are only interested in hilltops where we can assume sediment transport is linearly proportional to hillslope gradient. A second filter excluded hilltop vectors within 10 m of identified roads/trails/valley bottoms, any of which might influence slope and curvature estimates. The resulting network (Figure 5) was segmented to sample ridge sections with length >50 m to ensure that the number of sampled hillslopes equaled or exceeded 100 when averaging hillslope properties.

4.4. Sampling the Landscape

[23] We adopted two approaches to exploring how topography varies with erosion rates. CRN-derived denudation rates dictate a basin-averaged approach to allow direct

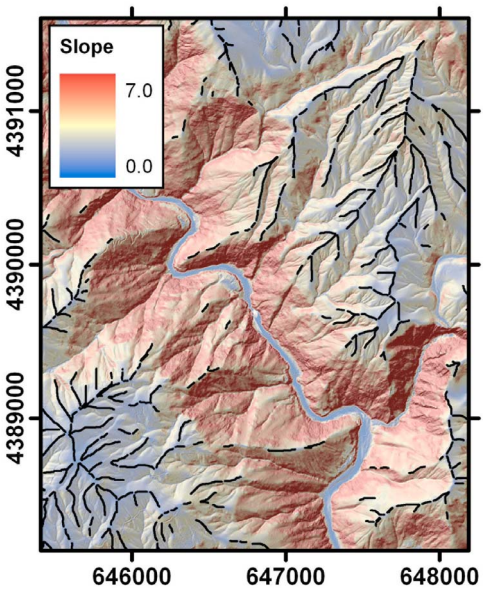

Figure 5. Shaded slope map adjacent to the Feather River canyon showing the network of mapped hilltops (black lines). Hilltops are defined at drainage divides where slope <0.4. Slope has units m/m. All slopes steeper than 1.0 appear red. The spatial reference system is UTM Zone 10N with spatial units in meters.

comparison between sampled topography (e.g., mean slope or mean hilltop curvature within a basin) and measured denudation. The second approach focused on the network of hilltop segments where topographic curvature was sampled only at locations defined as hilltops. Their adjacent hillslopes were sampled to determine mean slope, relief and hillslope length. Because a hilltop has two adjacent hillslopes and so is responding to erosion rates in two separate catchments, it follows that if there is a significant difference in erosion rates between catchments then the resulting hilltop curvature will be composite of the two erosion rates. In such a scenario a basin-averaged sampling approach may dampen or enhance the erosion rate inferred from curvature, since hilltops at the basin margin will reflect erosion rates in an adjacent basin as well as the basin of interest. While in section 4.2 we described methods for determining curvature throughout the landscape, we emphasize that the analysis described below samples this curvature only on mapped hilltops.

4.4.1. Basin-Averaged Sampling

[24] For comparison to CRN-derived denudation rates we extracted the mean slope of each sample basin [e.g., *Binnie et al.*, 2007; *Ouimet et al.*, 2009; *DiBiase et al.*, 2010; *Matsushi and Matsuzaki*, 2010]. No significant valley fill is observed in the landscape and therefore valleys were included in the analysis. Mean hilltop curvature was calculated from all hilltops internal to each basin. Hilltops at the basin margin were rejected if there was a noticeable difference in hillslope gradients either side of the divide. Catchment-averaged CRN-derived denudation rates rely on the assumption of spatially uniform denudation within the basin. In a transient scenario, steeper (adjusting) portions of the landscape are likely to contribute more sediment and thus CRN-derived denudation rates will be biased toward these portions of the landscape. For samples from the San Bernardino mountains [*Binnie et al.*, 2007], *DiBiase et al.* [2010] weight results for mean basin slope by estimates of

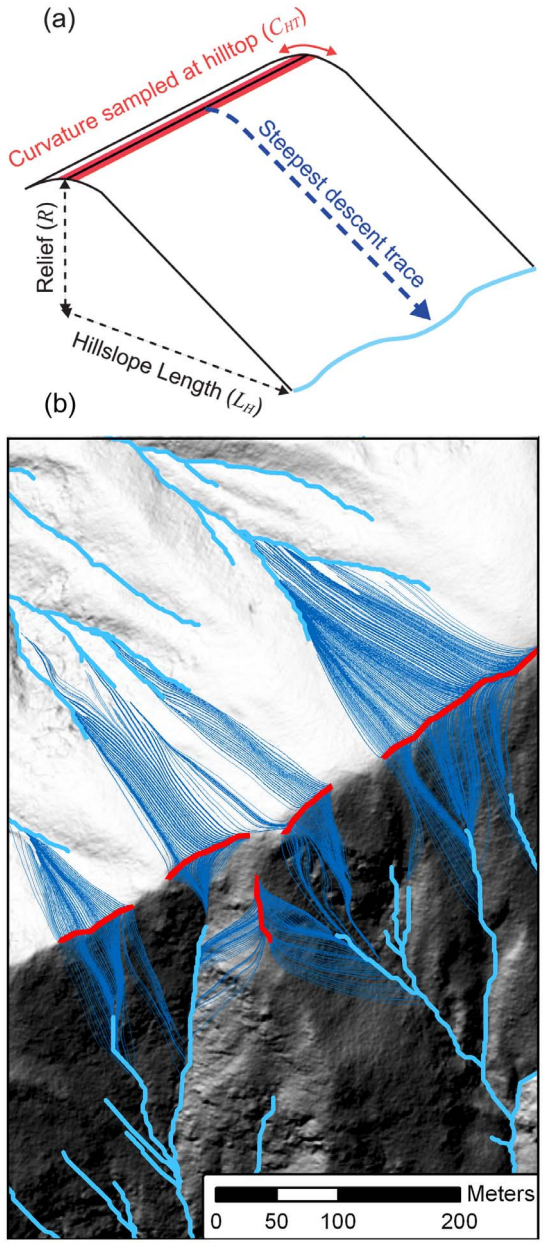

Figure 6. (a) Schematic illustration of sampling approach. For each digital elevation model pixel defined as a hilltop (red) the curvature was recorded (C_{HT}). A steepest descent path was generated until a stream pixel (light blue) was reached. The slope of each pixel encountered was collected and a mean (S) then calculated. From this trace hillslope length (L_H) and relief (R) were calculated. Mean values of each variable associated with each hilltop segment were calculated. (b) Sampling approach illustrated in Figure 6a applied to a real hillslope in the Feather River region showing a series of steepest descent traces between hilltops and valleys.

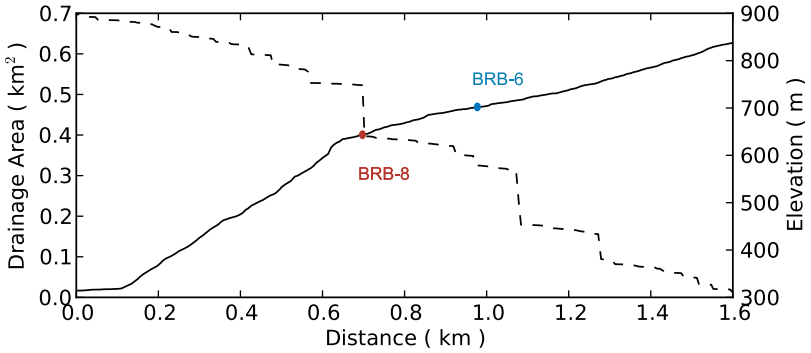

Figure 7. Long profile of a typical small basin immediately adjacent to the Feather River. Solid line is the elevation profile, and dashed line is drainage area along the channel. This basin is eroding at ~36 mm kyr^{-1} along its gentle upper reach upstream of the blue point (CRN sample BRB-6). Red point marks location where tributary eroding at ~90 mm kyr^{-1} joins (CRN sample BRB-8). The channel abruptly steepens as it approaches the rapidly incising Feather River, becoming linear and steep (mean slope 0.41), suggesting this is a hanging valley.

the total contribution of plateau and rejuvenated areas in the landscape to sediment flux in the basin. None of our samples were taken from parts of the landscape with such obvious boundaries in the terrain.

[25] For extracting basin averaged topographic metrics throughout the landscape we analyzed ~50,000 m^2 basins; large enough that there were some hilltops internal to the basin (i.e., not zero-order basins) but small enough that we could capture spatial variation in basin morphology.

4.4.2. Sampling Hillslopes

[26] To explore relationships between hillslope gradient and hilltop curvature throughout the landscape, algorithms were developed to extract hillslopes associated with each hilltop (Figures 6a and 6b). This approach is broadly similar to that of *Gangodagamage et al.* [2011]. For a given hilltop segment, beginning at each hilltop pixel, a trace was run down the path of steepest descent. The trace algorithm created a vector route which crosses a DEM pixel according to the aspect direction, and ran down pixel margins where two cells face each other [*Lea*, 1992]. The trace continued until a pixel defined as a valley bottom was reached. Along the resulting profile, the mean slope (S), relief (R) and horizontal hillslope length (L_H) were recorded. Hilltop curvature (C_{HT}) was recorded only at the top pixel (i.e., each trace that flows from the hilltop to the channel, is associated with a curvature measured only at

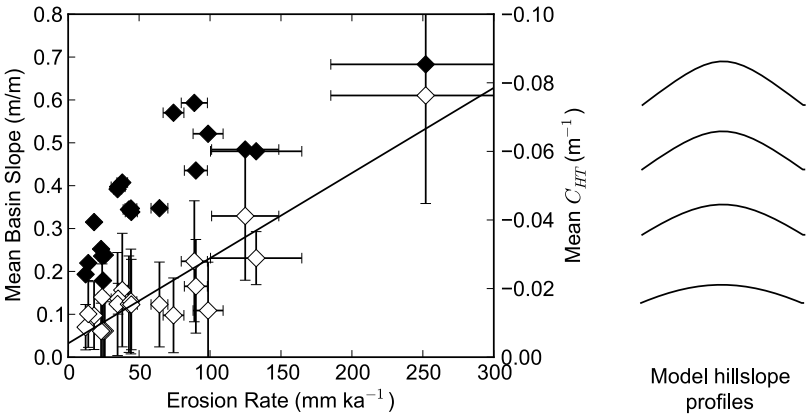

Figure 8. Plot showing variance of mean slope (filled diamonds) and mean hilltop curvature (hollow diamonds) with CRN-derived erosion rates for sampled basins (see Figure 2). Note that curvature (Laplacian) on convex-up hilltops is negative by convention, so "sharper" ridges have higher negative curvature. The linear relationship between erosion rate and hilltop curvature is predicted by equation (5), suggesting D = 0.0086 m^2 yr^{-1}. Error bars for hilltop curvature are one standard deviation about the mean. We do not include error bars for mean slope since we expect high variability in natural systems, but standard errors of the means are always smaller than the symbol plotted. Parabolas on the right represent steady state hillslope profiles (calculated following *Roering et al.* [2007] using D = 0.0086 m^2 y^{-1} and S_C = 0.80) to illustrate sharpening of ridges with increased erosion rate. These profiles have hilltop curvatures (from top to bottom) −0.08, −0.06, −0.04, and −0.02 m^{-1}, corresponding to the adjacent axis labels.

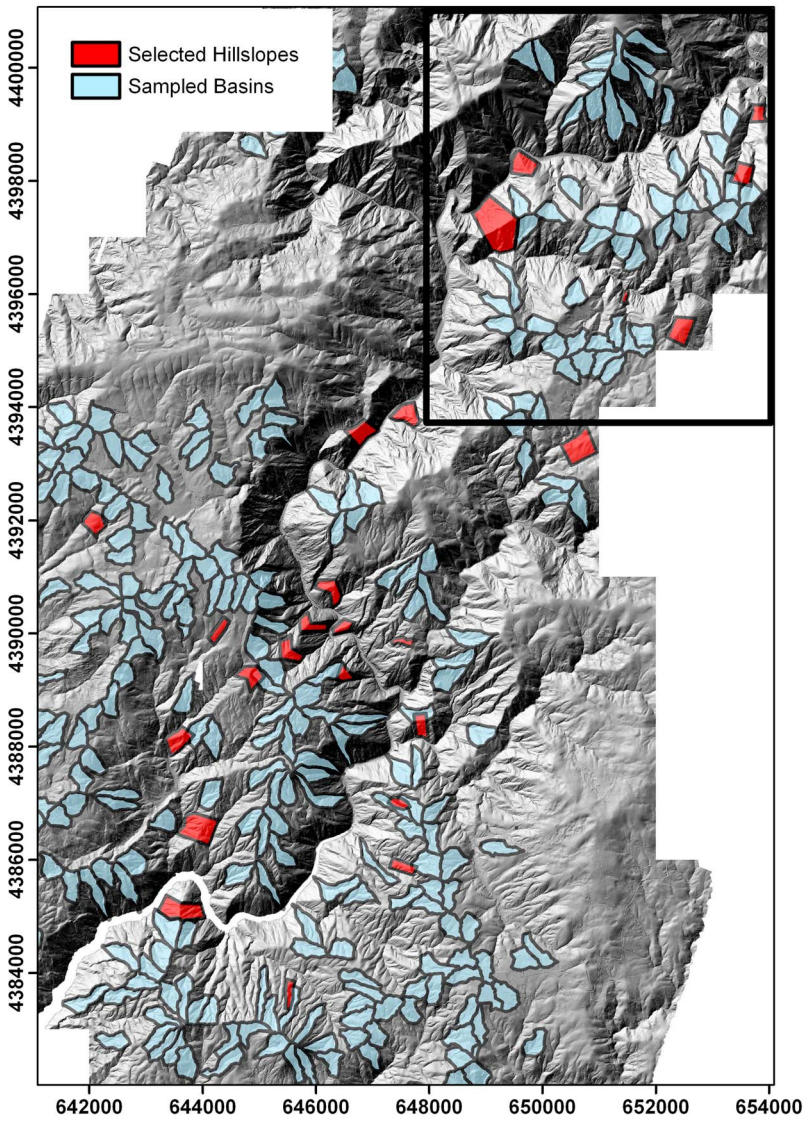

Figure 9. Shaded relief plot showing the location of all basins with a drainage area of 50,000 m^2 in granitoid basement and the location of hand selected ridges and their adjacent hillslopes used in Figure 10. The black box indicates the location shown in Figure 12. The spatial reference system is UTM Zone 10N with spatial units in meters.

the hilltop). A mean value for each of these metrics was then determined for each hilltop segment.

5. Results

5.1. CRN-Derived Denudation Rates and Topography

[27] *Riebe et al.* [2000] used cosmogenic radionuclides to demonstrate that erosion rates are an order of magnitude higher adjacent to the Feather River canyon, compared to rates on the relict upland. Here we recalculate denudation rates determined from $^{10}Be/^{9}Be$ ratios reported by *Riebe et al.* [2000] given new shielding factors [*Codilean*, 2006] and refinement in scaling of spallogenic and muogenic ^{10}Be production [e.g., *Dunai*, 2000; *Lifton et al.*, 2005]. We also calculate denudation rates for thirteen new catchments (Table 1). Denudation rates vary from 10 to 250 mm kyr^{-1} from the basins on the plateau to those immediately adjacent to the Feather River (Figure 2). There are three stages of landform evolution. Plateau erosion rates of 20–30 mm kyr^{-1} characterize the low-relief relict surface. In some locations slightly faster erosion rates ~30–40 mm kyr^{-1} are associated with a mature landscape cut into the plateau (concave-up channel profiles and broad convex up hillslopes). These areas are dissected because of accelerated erosion rates downstream, immediately adjacent to the Feather River, as indicated by knick zones and steepened reaches immediately upstream of the basin outlet (Figure 7). The intermediate zones between the plateau and the steepened landscape along the incised main rivers are common in the landscape and may be adjusted to a previous period of increased uplift prior to the late Cenozoic acceleration, as observed elsewhere in the Sierra Nevada [*Clark et al.*, 2005].

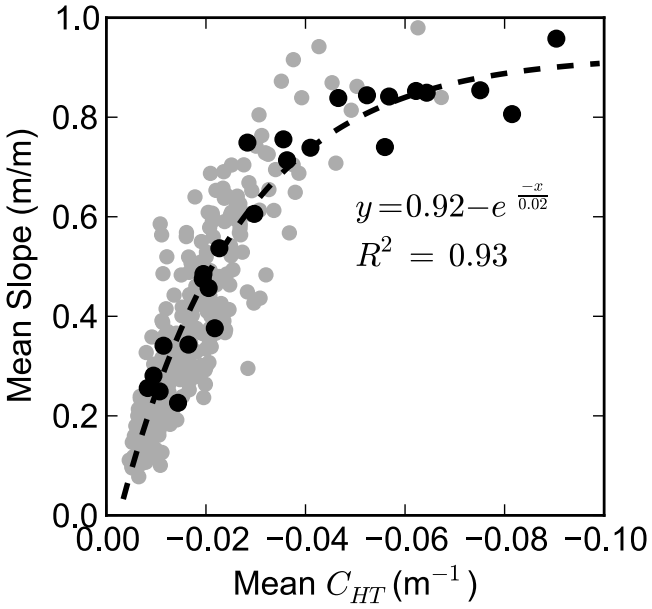

Figure 10. Relationships between topographic metrics of hilltop curvature and mean slope in areas sampled following Figure 9. A basin averaged sampling approach fails to sample hilltops with high curvature (gray circles), whereas sampling of ridges and their adjacent hillslopes reveals a nonlinear relationship as hillslope gradient becomes limited while hilltop curvature continues to increase (black circles). Dashed line represents least squares regression fit for an asymptote function.

[28] Figure 8 shows mean basin slope and mean hilltop curvature as a function of CRN-derived denudation rate. Mean basin slope is best approximated by a nonlinear curve (e.g., $R^2 = 0.78$ for asymptote compared to $R^2 = 0.69$ for linear fit) suggesting that hillslope angles are approaching some limited value with increasing denudation rates. This is conceptually consistent with the predictions of nonlinear sediment transport models suggesting that, as erosion rates increase, hillslopes may respond through an increasing frequency of mass wasting events [e.g., *Strahler*, 1950; *Burbank et al.*, 1996; *Roering et al.*, 1999]. If mean hilltop curvature varies linearly with denudation ($R^2 = 0.83$) then equation (5) is applicable to the landscape. However, an exponential function also provides a reasonable fit ($R^2 = 0.72$). We assume a linear fit is appropriate in order to use equation (5) to predict the coefficient of sediment transport, however there are theoretical reasons why this may not be the case in landscapes with thin soils [*Roering*, 2008] (see discussion).

5.2. Rates of Hillslope Sediment Transport

[29] On the basis of the regression line in Figure 8 we assume equation (5) is applicable throughout the landscape, and solve equation (5) for the transport coefficient D. Assuming $\rho_s/\rho_r = 0.5$, a ratio that has been demonstrated for other granitic field sites [e.g., *Heimsath et al.*, 2001; *Riggins et al.*, 2011], the transport coefficient is calibrated at $D = 0.0086$ m^2 yr^{-1} for areas of granitic bedrock lithology. Recognizing the dearth of data at erosion rates greater than $\sim$100 mm kyr^{-1} we performed the regression with the highest rate (FR-4, see Table 1) ignored and arrived at $D = 0.0077$ m^2 yr^{-1}.

5.3. Topographic Relationships Across the Entire Landscape

[30] We use our calibrated transport coefficient to predict erosion rates across the entire landscape by sampling hilltop segments and their associated adjacent hillslopes. Figure 9 shows basins that were sampled for topographic metrics, plus manually selected hilltop-hillslope areas (see below for rationale). A basin-averaged sampling approach failed to isolate rapidly eroding portions of the landscape, giving an approximately linear relationship between mean hilltop curvature and mean slope, and a dearth of data at high hilltop curvatures (Figure 10). The curvature of a hilltop is set by erosion rates in both adjacent channels. Rapidly eroding basins are limited spatially to being immediately adjacent to the Feather River, they are frequently adjacent to basins of lower relief. In such cases the mean curvature of hilltops at basin margins will be lower than the erosion rate in the basin should dictate. However, manual sampling of hilltops immediately adjacent to the Feather River, and their associated hillslopes, can focus on hilltops with steep planar hillslopes on both sides of the divide. For such hillslope areas shown in Figure 9, mean slope varies nonlinearly with hilltop curvature (Figure 10).

[31] Having automated the extraction of hilltops and adjacent hillslope properties, mean hilltop curvature and mean hillslope gradient were compared (Figure 11a). Hillslopes tend to steepen with increasing hilltop curvature but approach some limited value such that curvature can continue to increase without an obvious associated change in mean hillslope gradient. This relationship is highlighted by calculating average slope for regularly spaced bins in hilltop curvature. The transition to invariantly steep mean hillslope gradients with increasing hilltop curvature occurs gradually, in that as hilltop curvature increases slope angle becomes less sensitive to the change.

5.4. Comparison to Predictions of Geomorphic Transport Laws

[32] We compare our results to hillslope morphology predicted by hillslope sediment models (equations (7) and (8)) by calculating dimensionless erosion rate and dimensionless relief (Figure 11b). We also plot the distribution in predicted hillslope morphology for the nonlinear and threshold models for hillslope sediment transport (solid and dashed lines, equations (7) and (8), respectively). Using regularly spaced bins in dimensionless erosion rate (bin size = 1), we find our bin-averaged data offer a close fit to the nonlinear transport model (equation (7)) which predicts the transition to steep, planar hillslopes to be gradual rather than marked. This further suggests that equation (5) is applicable in this landscape, allowing us to predict the spatial distribution of erosion rates based on hilltop curvature (Figure 12).

6. Discussion

6.1. Steady State Assumption

[33] Given the assumptions that hillslope lowering (and therefore conversion of bedrock to soil) is approximately

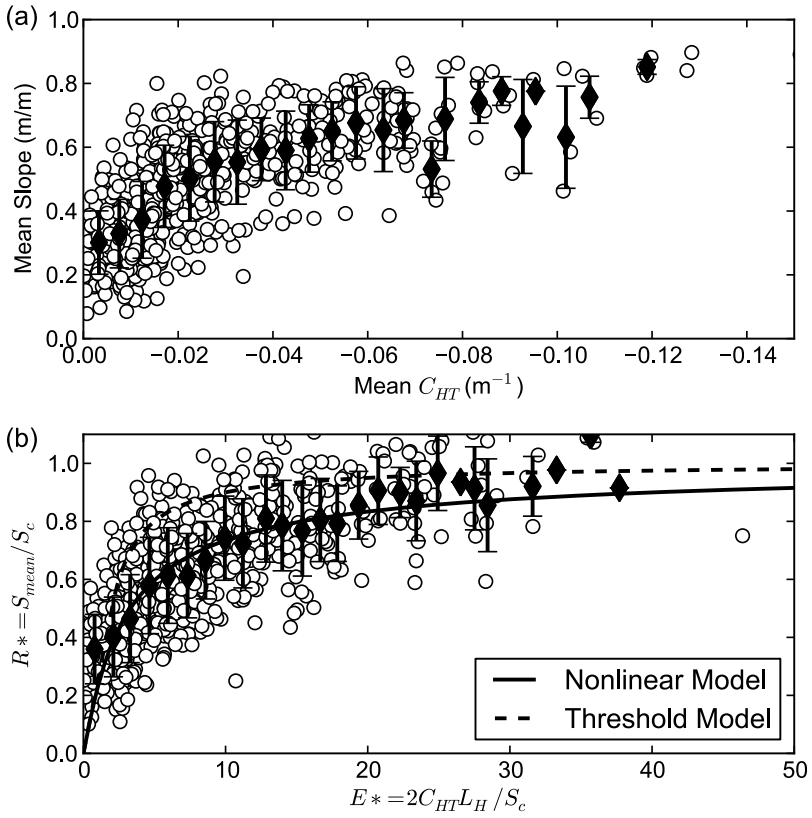

Figure 11. Topographic data generated by automated sampling of hilltops and their adjacent hillslopes. (a) Mean curvature versus mean slope for each hilltop segment and linearly spaced, binned averages (with ± 1 standard deviation bars). Slope increases linearly with hilltop curvature up to a curvature of ~ -0.03, beyond which slope appears to be less sensitive to changes in curvature. (b) Data from Figure 11a used to calculate dimensionless erosion rate and relief using measured hillslope lengths. Model predictions are shown for a nonlinear sediment flux model (equation (7)) and linear threshold model (equation (8)). Root-mean-square error is minimized between binned averages and the nonlinear model (equation (7)) using a critical slope $S_C = 0.80$.

uniform spatially and temporally (i.e., soil thickness and sediment flux are in steady state), and that sediment transport on hilltops is driven by creep-like processes, hilltop curvature can reveal the rates and distribution of erosion rates in a transient landscape at the scale of individual hillslopes. Our methods require that these assumptions be met on both sides of the topographic divide in question, since hillslope pixels distributed across the divide are required for the calculation of hilltop curvature. Critically, the application of hilltop curvature as a predictor of erosion rates requires the response time of hillslopes to be shorter than that of the fluvial network so that hilltops can track changes in channel erosion rates as they propagate through the landscape. We sought to verify this assumption since it is critical to the analysis presented in this study. A hilltop is the last part of the landscape to respond to a change in baselevel lowering, since the signal propagates up the channel network and onto the hillslopes. Hence the assumptions above are most likely to be violated on hillslopes which are coupled with the channel network immediately downstream of knickpoints, and the downstream extent of such transient hillslopes will be set by the velocity of knickpoint propagation and the response time of the hillslopes.

[34] Given our constraints on erosion rates and the transport coefficient, we can predict response times for a range of realistic hillslope lengths for our landscape. Following *Roering et al.* [2001b], the response time (t) can be calculated according to

$$t = -\tau \ln(P), \tag{10}$$

where P is a fraction set to define equilibrium and τ is an exponential timescale that defines how rapidly an equilibrium criterion approaches its asymptote [e.g., *Howard*, 1988]. For example consider a low-gradient ($S < 0.4$) hillslope responding to acceleration in erosion rate in the channel at its toe. The hillslope is expected to respond by increasing its relief. Using relief as a test criterion, by setting $P = 0.1$ we consider the hillslope to have reached equilibrium when relief has increased to 90% (1-P) of its final value. The exponential timescale τ is approximated by

$$\tau = \frac{{L_H}^2}{D} \frac{A}{(1+\psi)^B}, \tag{11}$$

where $A = 4/\pi^2$ [*Mudd and Furbish*, 2007], $B = 1.74 \pm 0.02$ is a constant [*Roering et al.*, 2001b] and ψ is the ratio of

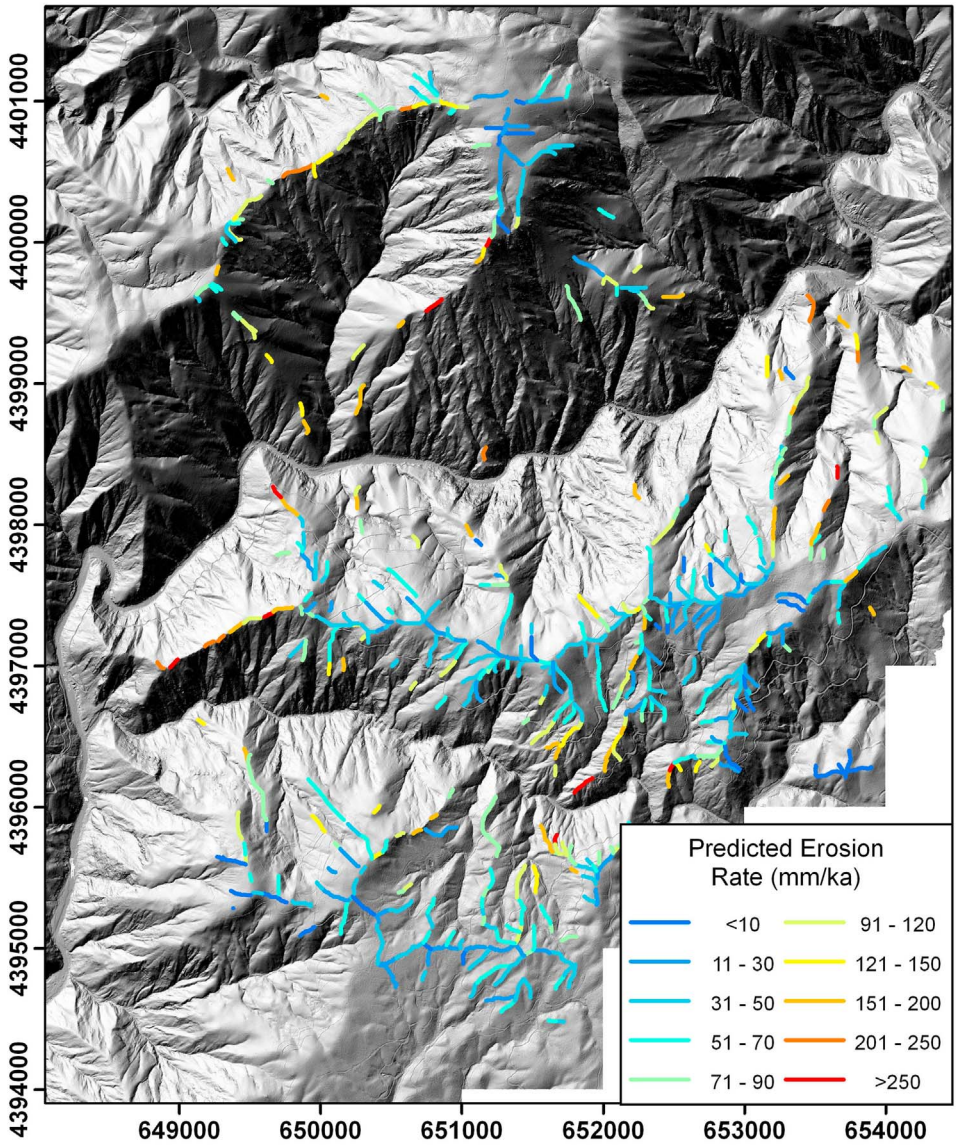

Figure 12. Shaded relief and hilltop map showing the spatial distribution of erosion rates predicted by hilltop curvature (using an estimated transport coefficient $D = 0.0086$ m^{2}yr^{-1}, $\rho_s/\rho_r = 0.5$). Curvature is elevated on hilltops near to the Feather River and its larger tributaries, where the fluvial network has transmitted the signal of increased erosion. The spatial reference system is UTM Zone 10N with spatial units in meters.

linear to nonlinear transport components at the hillslope toe when the hillslope is evolving according to equation (4). The response time of a soil-mantled hillslope is therefore primarily dependent on the length of the hillslope and the ratio of linear to nonlinear components of sediment transport, which is set by the erosion rate and transport coefficient D. The linear/nonlinear flux ratio can be described by

$$\psi = \frac{\left\{\frac{S_C}{2\varepsilon L_H}\left[-D + \sqrt{D^2 + \left(\frac{2\varepsilon L_H}{S_C}\right)^2}\right]\right\}}{1 - \left\{\frac{S_C}{2\varepsilon L_H}\left[-D + \sqrt{D^2 + \left(\frac{2\varepsilon L_H}{S_C}\right)^2}\right]\right\}}, \quad (12)$$

where $\varepsilon = E\ (\rho_r/\rho_s)$ (see the work of *Roering et al.* [2001b] for derivations). This equation predicts that as ψ increases (e.g., because of an increase in erosion rate), hillslope response time is reduced. It also predicts that the response time is further dependent on hillslope length. Figure 13 shows the predicted response timescales according to equation (11) for the range of hillslope lengths reported for our field site, within our constrained range of erosion rates. The response times for hillslopes given our calibrated parameters are predicted to be in the range 10–1000 kyr, which is shorter than typical response time for detachment limited rivers (typically several million years [*Whipple*, 2001; *Whittaker et al.*, 2007b; *Hobley et al.*, 2010]). The response time of the fluvial network in the Feather River

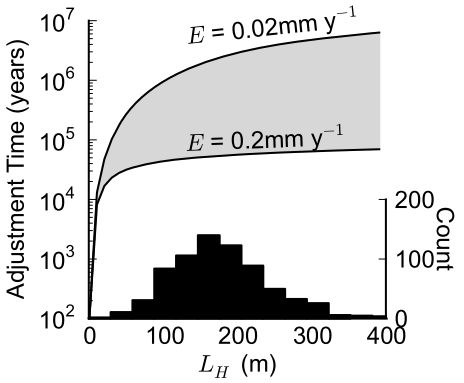

Figure 13. Predicted response timescales for hillslopes modeled using a nonlinear sediment flux law (equation (4); parameters used are D = 0.0086 m^2 yr^{-1}, S_C = 0.80), responding to a step increase in erosion rate. Response time decreases with increasing erosion rates and increases with hillslope length. For the range of measured erosion rates in this landscape, and the distribution of hillslope lengths (histogram), adjustment time ranges between 10 and 1000 kyr (gray). From this, given that erosion rates are increasing to ~250 mm kyr^{-1}, we expect the adjustment time in this landscape to be <100 kyr.

must be >5 Myr since the landscape has not fully responded yet to the perturbation initiated sometime since 5 Ma [e.g., *Wakabayashi and Sawyer*, 2001]. Yet, since erosion rates are increasing to ~250 mm kyr^{-1} hillslopes are expected to respond in less than 100 kyr (Figure 13). Hillslope response time is controlled by D and L_H such that longer hillslopes and less efficient sediment transport increase the response time (equation (11)). The transport of sediment is relatively efficient in the Feather River, shortening the response time experienced by a hillslope adjusting to an increase in erosion rate [*Fernandes and Dietrich*, 1997; *Roering et al.*, 2001b; *Mudd and Furbish*, 2007]. Consequently soil production and hilltop denudation should "catch up" with a new channel erosion rate relatively quickly, which is vital to the application of hilltop curvature for predicting erosion rates. *Roering et al.* [2001b] found a hillslope response time of ~50 kyr in the Oregon Coast Range, similar to the minimum response time indicated for the most frequent hillslope length in our landscape (Figure 13).

[35] Hillslope response is primarily driven by changes in the fluvial network; hence hillslopes will always lag behind transient signals in the channel network. However, since the hillslope relaxation time is short compared to that of the river network, hilltop curvature can offer insight into the distribution of erosion in the channel network. The approach taken in this study is dependent on hillslopes being able to respond relatively rapidly to a change in incision rate at the toe of the hillslope. This response timescale will dictate the spatial extent of hillslopes whose morphology does not reflect channel erosion (Figure 15). Where hillslopes are unable to keep pace with channel incision, the hillslope may be effectively decoupled from the channel network [e.g., *Korup and Schlunegger*, 2007; *Norton et al.*, 2008], and hilltop curvature will bear no relation to erosion rates in the channel.

[36] Hillslope response times calculated here are significantly greater than timescales over which climate is considered to vary. Climatic variability is thought to control the efficiency of sediment transport on hillslopes through changing the type and distribution of biota, the amount of moisture in the soil and the length of winters and growing seasons. The style and timescale of hillslope response to climate fluctuations remains poorly understood [*Roering et al.*, 2007; *Tucker et al.*, 2011].

[37] The assumption of steady state is also critical to the application of CRN to determine basin-averaged denudation. Most critically, denudation in the basin must be assumed spatially and temporally constant for the period over which denudation rate is calculated. Where the basin is still responding to acceleration in channel incision, sediment with a ^{10}Be inventory indicative of the previous, slower erosional regime may contribute to the measured signal until the basin is fully adjusted. *Bierman and Steig* [1996] demonstrate that such heterogeneity should not mask a basin averaged erosion rate. However, the stochastic nature of landsliding may result in the mobilization and contribution of sediment with low ^{10}Be inventories from well below the surface, which could result in overestimated erosion rates in small catchments [*Niemi et al.*, 2005].

6.2. Comparison to Other Topographic Metrics

[38] Our new technique for mapping the spatial distribution of erosion rates across a landscape not only predicts erosion rates above those at which mean hillslope angles become insensitive, but also allows prediction of rates at the scale of a single hillslope portion. The use of normalized steepness indices in the channel network is reliant on a basin-averaged sampling approach in basins large enough that it can be confidently assumed that fluvial processes are the dominant valley forming process. Many of the Feather River's tributary valleys might be described as hanging valleys [e.g., *Wobus et al.*, 2006b; *Crosby et al.*, 2007] and are effectively decoupled from erosion rates in the main Feather River (Figure 7). Valley profiles are commonly planar approaching their outlet, exhibiting slopes >0.4. As such, the valley forming process may not be fluvial, but rather debris flow dominated [e.g., *Sklar and Dietrich*, 1998; *Stock and Dietrich*, 2006].

[39] All topographic metrics currently used to infer erosion rates cease to predict rates above some limited value. Invariantly steep, planar hillslopes emerge when erosion rates exceed ~200–300 mm kyr^{-1} [e.g., *Binnie et al.*, 2007; *DiBiase et al.*, 2010]. Such limits are probably dependent on lithology and climate. In our landscape the transition may occur at erosion rates as low as ~150 mm kyr^{-1} (Figure 8) yet the landscape remains predominantly forested and soil mantled. Normalized channel steepness indices may allow inference of higher erosion rates, possibly up to 600 mm kyr^{-1}, but also seem to be limited [*Ouimet et al.*, 2009], perhaps by down-valley extension of debris flow dominated erosion. In order to use hilltop curvature to predict erosion rates, a hilltop must be soil-mantled such that creep-like processes (e.g., expansion-contraction, freeze-thaw, root growth-decay, tree throw) can be assumed to be the dominant conveyor of soil. Therefore the application of techniques described in this contribution is limited to landscapes where erosion rates do not exceed the maximum soil production

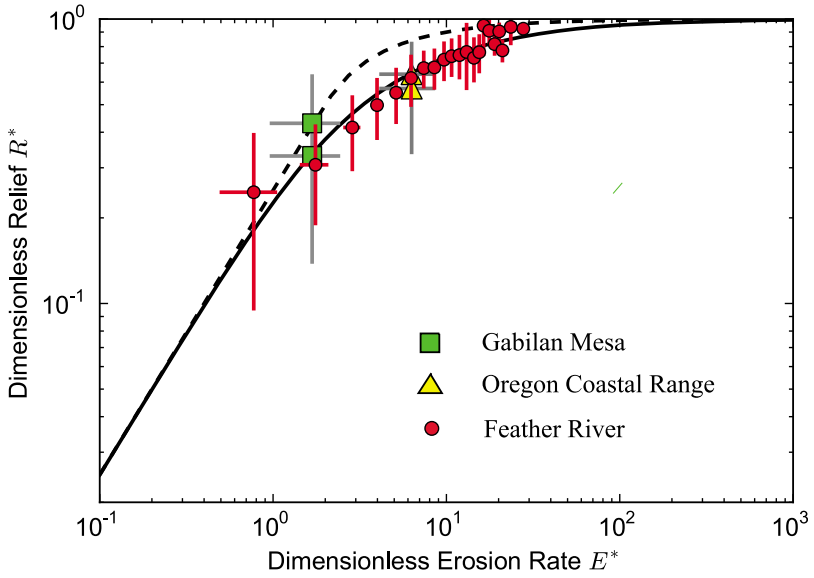

Figure 14. Modeled relationship between dimensionless erosion rate and dimensionless hillslope relief predicted by equations (7) (solid) and (8) (dashed). Plot shows results reported by *Roering et al.* [2007] for Gabilan Mesa (green) and Oregon Coastal Range (yellow). Results from the Feather River (red) span a range of erosion rates and relief.

rates on hilltops. In our field site, soils are present on slopes where hilltop curvatures approach $C_{HT} = -0.08$, suggesting soils can persist in this landscape at erosion rates as high as 250 mm kyr^{-1}. Others have reported maximum soil production rates in the range 200–400 mm kyr^{-1} [e.g., *DiBiase et al.*, 2010; *Heimsath et al.*, 2012]. In addition, some soil production mechanisms, such as overturning of bedrock during tree throw, appear to be able to maintain a patchy soil cover at high erosion rates (∼500 mm kyr^{-1}) [*Gabet and Mudd*, 2010; *Heimsath et al.*, 2012]. Given that hilltops in some rapidly eroding terrain are able to retain a patchy soil mantle, we feel that the mechanisms of soil production in such landscapes, particularly on ridges, require further investigation [e.g., *Roering et al.*, 2010]. Our results highlight that the maximum soil production rate (>250 mm kyr^{-1}) may not necessarily coincide with the erosion rate at which hillslope gradients become limited (100–150 mm kyr^{-1}) as suggested by *Heimsath et al.* [2012]. It is the ability of soil production on hilltops to keep pace with erosion rates which is critical to the outcomes of this study. Given this result, analysis of in situ CRN sampled in soil on hilltops would allow direct comparison of soil production rates to hilltop curvature to further test the results presented here.

[40] We have restricted our analyses to portions of the landscape where hilltops were observed to be soil mantled. However, there are significant bedrock exposures within the part of the landscape underlain by granitoids. These occur either (1) in broad patches on the gently eroding relict surface or (2) immediately adjacent to the Feather River, in large single patches of exposure below the break in slope separating the steepened landscape from the relict topography. This may be attributed to particularly resistant patches of granitoid and/or a negative feedback whereby stripping of soil inhibits further soil production. The conversion of bedrock to soil follows a "humped" function with soil production dependent on soil depth. Above some optimal soil thickness at which soil production is highest, soil production rate declines exponentially with soil depth [e.g., *Heimsath et al.*, 1997]. The maximum attainable soil production rate is itself dependent on erosion rate [*Heimsath et al.*, 2012]. Yet in order to convert bedrock to soil, a covering soil layer is required to trap water and allow plant colonization [e.g., *Wilkinson et al.*, 2005; *Gabet and Mudd*, 2010]. When soil becomes too thin or is removed altogether, bedrock hillslopes will emerge. Sediment flux may have some dependence on soil depth [e.g., *Mudd and Furbish*, 2007; *Roering*, 2008] in which case any relationship between hilltop curvature and erosion rates may be nonlinear. However, soil depths measured in the Feather River do not depend on erosion rate and the depth of sediment transport penetration seems to be set by the rooting depth of the vegetation [*Yoo et al.*, 2011]. Such conditions are more likely to be approximated by equation (4).

[41] The application of hilltop curvature, in concert with other topographic metrics for erosion rate such as channel steepness indices [e.g., *DiBiase et al.*, 2010] will allow for comparison of predicted erosion rates at different scales within landscapes. Additionally this may provide insight into the scale of spatial heterogeneity in erosion rates in both steady state and transiently adjusting landscapes.

6.3. Influence of Landscape Transience

[42] Many tributary basins in our field setting contain steepened reaches immediately upstream of their outlet into the Feather River (Figure 7). Such hanging valleys [e.g., *Wobus et al.*, 2006b; *Crosby et al.*, 2007] prevent the most recent tectonic signal and subsequent increase in erosion rate from being "felt" by parts of the landscape upstream of the oversteepened reach. The result is that very few hilltops adjacent to the Feather River are being forced by the new incision rate in the channels that flank them on both sides. Hilltops with hillslopes responding to the new incision rates

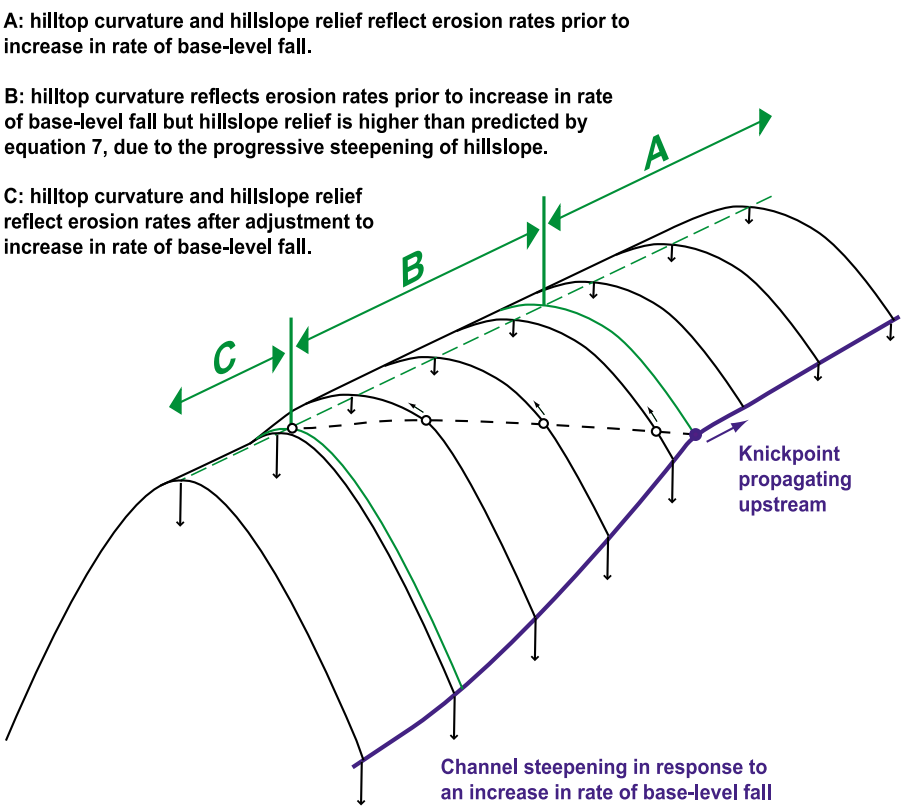

Figure 15. Schematic illustrating the predicted response of the landscape to an increase in the rate of base level fall. A knickpoint propagates upstream along the channel, separating the steepened landscape from the relict topography. In response to the increase in erosion rate along the channel, a wave of increasing slope and surface lowering propagates up the hillslopes (dots with black arrows), leading to the alteration of the relationship between hilltop curvature and hillslope relief and the differentiation of three domains (A, B, and C). The width of domain B is a function of the response time of the hillslopes (the shorter the response time, the narrower the domain B).

on both sides are restricted to areas dividing the Feather River from a large tributary, with close proximity to the Feather River itself. Previous quantification of dimensionless erosion rate and relief have focused in landscapes that can be assumed to be at topographic steady state [*Roering et al.*, 2007], but despite landscape transience, hillslope morphology in the Feather River closely matches theoretical predictions (Figure 14).

[43] The transient state of the Feather River is an important consideration in the interpretation of our findings. Consider, in this regard, a mature hillslope responding to an increase in erosion rate. This transience will be first manifest as an increase in slope at the toe of the hillslope, resulting in increased sediment flux. A wave of increasing slope will propagate from the toe to the divide with associated responses in soil thickness and production rates [*Roering et al.*, 2001b; *Mudd and Furbish*, 2005]. Such a transient hillslope is therefore predicted to deviate from model predictions (equation (7)) since its slope may increase while its hilltop curvature remains constant, plotting above the line predicted by equation (7) (Figure 15). These criteria may allow us to identify the spatial distribution of transient or adjusting portions of the landscape in future contributions (Figure 15). Such transient relationships may be increasing the apparent nonlinearity between hilltop curvature and slope angles in Figure 11a if there are a significant number of hilltops with elevated slopes and low hilltop curvature. Given our estimates for the response time of hillslopes, we would expect there to be significant portions of the landscape still undergoing adjustment.

7. Conclusions

[44] The topographic form of hillslopes in a landscape undergoing a transient response to a rapid drop in base level can be quantified through the extraction of hilltops and their adjacent hillslopes. Our study shows that (negative) hilltop curvature increases with CRN-derived erosion rates varying over an order of magnitude (20–250 mm kyr^{-1}). The suggested linear nature of this relationship facilitates calibration of the transport coefficient, allowing denudation rates to be predicted across the landscape using hilltop curvature. Following the framework of *Roering et al.* [2007], the distribution and covariance of hilltop curvature and slope angles appear to best replicate hillslope evolution models in which the transition from creep-dominated to landslide-dominated hillslopes is continuous and gradual, rather than a threshold model. In landscapes where hillslopes can respond relatively

quickly to adjustment in the channel network, if the efficiency of sediment transport on hillslopes can be estimated, hilltop curvature can be used to predict erosion rates at the scale of individual hillslopes.

[45] **Acknowledgments.** This work was supported by a National Environment Research Council doctoral training grant NE/G524128/1 awarded to M. Hurst. Funding for this work was also provided by the National Science Foundation EAR0819064 (Empirical and Theoretical Integration of Geochemical and Morphologic Evolution of Soil-Covered Hillslopes: Responses to Channel Incision) to K. Yoo and S.M. Mudd for which lidar topographic data was acquired by the National Center for Airborne Laser Mapping. Additional funding was provided by the Natural Environment Research Council (NE/H001174/1) to S.M. Mudd. We are grateful to Beth Weinman for her insights and comments, and wish to thank Kate Maher and Kristin Mayer for assistance in the field. Ben Crosby, the Editor, Assistant Editor, and four anonymous reviewers provided comments and insights which allowed us to substantially improve the manuscript.

References

Ahnert, F. (1970), Functional relationships between denudation, relief, and uplift in large mid-latitude drainage basins, *Am. J. Sci.*, *268*(3), 243–263, doi:10.2475/ajs.268.3.243.

Andrews, D. J., and R. C. Bucknam (1987), Fitting degradation of shoreline scarps by a nonlinear diffusion model, *J. Geophys. Res.*, *92*(B12), 12,857–12,867, doi:10.1029/JB092iB12p12857.

Attal, M., P. A. Cowie, A. C. Whittaker, D. Hobley, G. E. Tucker, and G. P. Roberts (2011), Testing fluvial erosion models using the transient response of bedrock rivers to tectonic forcing in the Apennines, Italy, *J. Geophys. Res.*, *116*, F02005, doi:10.1029/2010JF001875.

Balco, G., J. O. Stone, N. A. Lifton, and T. J. Dunai (2008), A complete and easily accessible means of calculating surface exposure ages or erosion rates from ^{10}Be and ^{26}Al measurements, *Quat. Geochronol.*, *3*(3), 174–195, doi:10.1016/j.quageo.2007.12.001.

Bierman, P., and E. J. Steig (1996), Estimating rates of denudation using cosmogenic isotope abundances in sediment, *Earth Surf. Processes Landforms*, *21*(2), 125–139, doi:10.1002/(SICI)1096-9837(199602)21:2<125::AID-ESP511>3.0.CO;2-8.

Bierman, P. R., M. C. Caffee, P. T. Davis, K. Marsella, M. Pavich, P. Colgan, D. Mickelson, and J. Larsen (2002), Rates and timing of Earth surface processes from in situ–produced cosmogenic ^{10}Be, in *Beryllium: Mineralogy, Petrology, and Geochemistry*, *Rev. Mineral. Geochem.*, vol. 50, edited by E. Grew, pp. 147–205, doi:10.2138/rmg.2002.50.4, Mineral. Soc. of Am., Washington, D. C.

Binnie, S. A., W. M. Phillips, M. A. Summerfield, and L. K. Fifield (2007), Tectonic uplift, threshold hillslopes, and denudation rates in a developing mountain range, *Geology*, *35*(8), 743–746, doi:10.1130/G23641A.1.

Brown, E. T., R. F. Stallard, M. C. Larsen, G. M. Raisbeck, and F. Yiou (1995), Denudation rates determined from the accumulation of in situ–produced ^{10}Be in the luquillo experimental forest, Puerto Rico, *Earth Planet. Sci. Lett.*, *129*(1–4), 193–202, doi:10.1016/0012-821X(94)00249-X.

Burbank, D. W., J. Leland, E. Fielding, R. S. Anderson, N. Brozovic, M. R. Reid, and C. Duncan (1996), Bedrock incision, rock uplift and threshold hillslopes in the northwestern Himalayas, *Nature*, *379*(6565), 505–510, doi:10.1038/379505a0.

Busby, C. J., and K. Putirka (2009), Miocene evolution of the western edge of the Nevadaplano in the central and northern Sierra Nevada: Palaeocanyons, magmatism, and structure, *Int. Geol. Rev.*, *51*(7–8), 670–701, doi:10.1080/00206810902978265.

Cecil, M. R., M. N. Ducea, P. W. Reiners, and C. G. Chase (2006), Cenozoic exhumation of the northern Sierra Nevada, California, from (U-Th)/He thermochronology, *Geol. Soc. Am. Bull.*, *118*(11–12), 1481–1488, doi:10.1130/B25876.1.

Clark, D. H. (1995), Extent, timing, and climatic significance of latest Pleistocene and Holocene glaciation in the Sierra Nevada, California, PhD thesis, 193 pp., Univ. of Wash., Seattle.

Clark, M. K., G. Maheo, J. Saleeby, and K. A. Farley (2005), The non-equilibrium landscape of the southern Sierra Nevada, California, *GSA Today*, *15*(9), 4–10, doi:10.1130/1052-5173(2005)015[4:TNLOTS]2.0.CO;2.

Codilean, A. T. (2006), Calculation of the cosmogenic nuclide production topographic shielding scaling factor for large areas using DEMs, *Earth Surf. Processes Landforms*, *31*(6), 785–794, doi:10.1002/esp.1336.

Cowie, P. A., A. C. Whittaker, M. Attal, G. P. Roberts, G. E. Tucker, and A. Ganas (2008), New constraints on sediment-flux-dependent river incision: Implications for extracting tectonic signals from river profiles, *Geology*, *36*(7), 535–538, doi:10.1130/G24681A.1.

Crosby, B. T., K. X. Whipple, N. M. Gasparini, and C. W. Wobus (2007), Formation of fluvial hanging valleys: Theory and simulation, *J. Geophys. Res.*, *112*, F03S10, doi:10.1029/2006JF000566.

Culling, W. E. H. (1960), Analytical theory of erosion, *J. Geol.*, *68*(3), 336–344, doi:10.1086/626663.

Cyr, A. J., D. E. Granger, V. Olivetti, and P. Molin (2010), Quantifying rock uplift rates using channel steepness and cosmogenic nuclide-determined erosion rates: Examples from northern and southern Italy, *Lithosphere*, *2*(3), 188–198, doi:10.1130/L96.1.

Daly, C., G. Taylor, and W. Gibson (1997), The PRISM approach to mapping precipitation and temperature, paper presented at 10th Conference on Applied Climatology, Am. Meteorol. Soc., Reno, Nev.

Davis, W. M. (1892), The convex profile of badland divides, *Science*, *20*, 245, doi:10.1126/science.ns-20.508.245.

Day, H. W., and M. E. Bickford (2004), Tectonic setting of the Jurassic Smartville and Slate Creek complexes, northern Sierra Nevada, California, *Geol. Soc. Am. Bull.*, *116*(11–12), 1515–1528, doi:10.1130/B25416.1.

Densmore, A. L., M. A. Ellis, and R. S. Anderson (1998), Landsliding and the evolution of normal-fault-bounded mountains, *J. Geophys. Res.*, *103*(B7), 15,203–15,219, doi:10.1029/98JB00510.

DiBiase, R. A., and K. X. Whipple (2011), The influence of erosion thresholds and runoff variability on the relationships among topography, climate, and erosion rate, *J. Geophys. Res.*, *116*, F04036, doi:10.1029/2011JF002095.

DiBiase, R. A., K. X. Whipple, A. M. Heimsath, and W. B. Ouimet (2010), Landscape form and millennial erosion rates in the San Gabriel Mountains, CA, *Earth Planet. Sci. Lett.*, *289*(1–2), 134–144, doi:10.1016/j.epsl.2009.10.036.

DiBiase, R. A., A. M. Heimsath, and K. X. Whipple (2012), Hillslope response to tectonic forcing in threshold landscapes, *Earth Surf. Processes Landforms*, doi:10.1002/esp.3205, in press.

Dietrich, W. E., D. G. Bellugi, L. S. Sklar, and J. D. Stock (2003), Geomorphic transport laws for predicting landscape form and dynamics, in *Prediction in Geomorphology*, *Geophys. Monogr. Ser*, vol. 135, edited by P. R. Wilcock and R. M. Iverson, pp. 103–132, AGU, Washington, D. C., doi:10.1029/135GM09.

Dunai, T. J. (2000), Scaling factors for production rates of in situ produced cosmogenic nuclides: A critical reevaluation, *Earth Planet. Sci. Lett.*, *176*(1), 157–169, doi:10.1016/S0012-821X(99)00310-6.

Evans, I. S. (1980), An integrated system of terrain analysis and slope mapping, *Z. Geomorphol.*, *36*, 274–295.

Fernandes, N. F., and W. E. Dietrich (1997), Hillslope evolution by diffusive processes: The timescale for equilibrium adjustments, *Water Resour. Res.*, *33*(6), 1307–1318, doi:10.1029/97WR00534.

Finnegan, N. J., G. Roe, D. R. Montgomery, and B. Hallet (2005), Controls on the channel width of rivers: Implications for modeling fluvial incision of bedrock, *Geology*, *33*(3), 229–232, doi:10.1130/G21171.1.

Foufoula-Georgiou, E., V. Ganti, and W. Dietrich (2010), A nonlocal theory of sediment transport on hillslopes, *J. Geophys. Res.*, *115*, F00A16, doi:10.1029/2009JF001280.

Gabet, E. J. (2000), Gopher bioturbation: Field evidence for non-linear hillslope diffusion, *Earth Surf. Processes Landforms*, *25*(13), 1419–1428, doi:10.1002/1096-9837(200012)25:13<1419::AID-ESP148>3.0.CO;2-1.

Gabet, E. J., and S. M. Mudd (2010), Bedrock erosion by root fracture and tree throw: A coupled biogeomorphic model to explore the humped soil production function and the persistence of hillslope soils, *J. Geophys. Res.*, *115*, F04005, doi:10.1029/2009JF001526.

Gangodagamage, C., P. Belmont, and E. Foufoula-Georgiou (2011), Revisiting scaling laws in river basins: New considerations across hillslope and fluvial regimes, *Water Resour. Res.*, *47*, W07508, doi:10.1029/2010WR009252.

Gilbert, G. K. (1877), *Report on the Geology of the Henry Mountains*, 160 pp., U.S. Gov. Print. Off., Washington, D. C.

Gilbert, G. K. (1909), The convexity of hilltops, *J. Geol.*, *17*(4), 344–350, doi:10.1086/621620.

Gosse, J. C., and F. M. Phillips (2001), Terrestrial in situ cosmogenic nuclides: Theory and application, *Quat. Sci. Rev.*, *20*(14), 1475–1560, doi:10.1016/S0277-3791(00)00171-2.

Granger, D. E., J. W. Kirchner, and R. Finkel (1996), Spatially averaged long-term erosion rates measured from in situ–produced cosmogenic nuclides in alluvial sediment, *J. Geol.*, *104*(3), 249–257, doi:10.1086/629823.

Heimsath, A. M., W. E. Dietrich, K. Nishiizumi, and R. C. Finkel (1997), The soil production function and landscape equilibrium, *Nature*, *388*(6640), 358–361, doi:10.1038/41056.

Heimsath, A. M., J. Chappell, W. E. Dietrich, K. Nishiizumi, and R. C. Finkel (2001), Late Quaternary erosion in southeastern Australia: A field

example using cosmogenic nuclides, *Quat. Int.*, *83–85*, 169–185, doi:10.1016/S1040-6182(01)00038-6.

Heimsath, A. M., R. A. DiBiase, and K. X. Whipple (2012), Soil production limits and the transition to bedrock-dominated landscapes, *Nat. Geosci.*, *5*, 210–214, doi:10.1038/NGEO1380.

Hobley, D. E. J., H. D. Sinclair, and P. A. Cowie (2010), Processes, rates, and time scales of fluvial response in an ancient postglacial landscape of the northwest Indian Himalaya, *Geol. Soc. Am. Bull.*, *122*(9–10), 1569–1584, doi:10.1130/B30048.1.

Howard, A. D. (1988), Equilibrium models in geomorphology, in *Modelling Geomorphological Systems*, edited by M. G. Anderson, pp. 49–72, John Wiley, New York.

Howard, A. D. (1994), A detachment-limited model of drainage-basin evolution, *Water Resour. Res.*, *30*(7), 2261–2285, doi:10.1029/94WR00757.

Jones, C. H., G. L. Farmer, and J. Unruh (2004), Tectonics of Pliocene removal of lithosphere of the Sierra Nevada, California, *Geol. Soc. Am. Bull.*, *116*(11–12), 1408–1422, doi:10.1130/B25397.1.

Kirby, E., and W. Ouimet (2011), Tectonic geomorphology along the eastern margin of Tibet: Insights into the pattern and processes of active deformation adjacent to the Sichuan Basin, *Spec. Publ. Geol. Soc.*, *353*, 165–188, doi:10.1144/SP353.9.

Kirby, E., K. X. Whipple, W. Tang, and Z. Chen (2003), Distribution of active rock uplift along the eastern margin of the Tibetan Plateau: Inferences from bedrock channel longitudinal profiles, *J. Geophys. Res.*, *108*(B4), 2217, doi:10.1029/2001JB000861.

Kirby, E., C. Johnson, K. Furlong, and A. Heimsath (2007), Transient channel incision along Bolinas Ridge, California: Evidence for differential rock uplift adjacent to the San Andreas fault, *J. Geophys. Res.*, *112*, F03S07, doi:10.1029/2006JF000559.

Korup, O., and F. Schlunegger (2007), Bedrock landsliding, river incision, and transience of geomorphic hillslope-channel coupling: Evidence from inner gorges in the Swiss Alps, *J. Geophys. Res.*, *112*, F03027, doi:10.1029/2006JF000710.

Lashermes, B., E. Foufoula-Georgiou, and W. E. Dietrich (2007), Channel network extraction from high resolution topography using wavelets, *Geophys. Res. Lett.*, *34*, L23S04, doi:10.1029/2007GL031140.

Lea, N. J. (1992), An aspect-driven kinematic routing algorithm, in *Overland Flow: Hydraulics and Erosion Mechanics*, edited by A. J. Parsons and A. D. Abrahams, pp. 393–407, U. C. L. Press, London.

Lifton, N. A., J. W. Bieber, J. M. Clem, M. L. Duldig, P. Evenson, J. E. Humble, and R. Pyle (2005), Addressing solar modulation and long-term uncertainties in scaling secondary cosmic rays for in situ cosmogenic nuclide applications, *Earth Planet. Sci. Lett.*, *239*, 140–161, doi:10.1016/j.epsl.2005.07.001.

Matsushi, Y., and H. Matsuzaki (2010), Denudation rates and threshold slope in a granitic watershed, central Japan, *Nucl. Instrum. Methods Phys. Res., Sect. B*, *268*(7–8), 1201–1204, doi:10.1016/j.nimb.2009.10.133.

Montgomery, D. R. (2001), Slope distributions, threshold hillslopes, and steady-state topography, *Am. J. Sci.*, *301*(4–5), 432–454, doi:10.2475/ajs.301.4-5.432.

Montgomery, D. R., and M. T. Brandon (2002), Topographic controls on erosion rates in tectonically active mountain ranges, *Earth Planet. Sci. Lett.*, *201*(3–4), 481–489, doi:S0012821X02007252.

Moore, I. D., R. B. Grayson, and A. R. Ladson (1991), Digital terrain modeling: A review of hydrological, geomorphological, and biological applications, *Hydrol. Processes*, *5*(1), 3–30, doi:10.1002/hyp.3360050103.

Mudd, S. M., and D. J. Furbish (2004), Influence of chemical denudation on hillslope morphology, *J. Geophys. Res.*, *109*, F02001, doi:10.1029/2003JF000087.

Mudd, S. M., and D. J. Furbish (2005), Lateral migration of hillcrests in response to channel incision in soil-mantled landscapes, *J. Geophys. Res.*, *110*, F04026, doi:10.1029/2005JF000313.

Mudd, S. M., and D. J. Furbish (2007), Responses of soil-mantled hillslopes to transient channel incision rates, *J. Geophys. Res.*, *112*, F03S18, doi:10.1029/2006JF000516.

National Operational Hydrologic Remote Sensing Center (2004), Snow Data Assimilation System (SNODAS) data products at NSIDC, http://nsidc.org/data/docs/noaa/g02158_snodas_snow_cover_model/index.html, Natl. Snow and Ice Data Cent., Boulder, Colo., 3 March 2011.

Niemi, N. A., M. Oskin, D. W. Burbank, A. M. Heimsath, and E. J. Gabet (2005), Effects of bedrock landslides on cosmogenically determined erosion rates, *Earth Planet. Sci. Lett.*, *237*(3–4), 480–498, doi:10.1016/j.epsl.2005.07.009.

Nishiizumi, K., M. Imamura, M. Caffee, J. Southon, R. Finkel, and J. McAnich (2007), Absolute calibration of ^{10}Be AMS standards, *Nucl. Instrum. Methods Phys. Res., Sect. B*, *258*, 403–413, doi:10.1016/j.nimb.2007.01.297.

Norton, K. P., F. von Blanckenburg, F. Schlunegger, M. Schwab, and P. W. Kubik (2008), Cosmogenic nuclide-based investigation of spatial erosion and hillslope channel coupling in the transient foreland of the Swiss Alps, *Geomorphology*, *95*, 474–486, doi:10.1016/j.geomorph.2007.07.013.

Ouimet, W. B., K. X. Whipple, and D. E. Granger (2009), Beyond threshold hillslopes: Channel adjustment to base-level fall in tectonically active mountain ranges, *Geology*, *37*(7), 579–582, doi:10.1130/G30013A.1.

Palumbo, L., R. Hetzel, M. Tao, and X. Li (2010), Topographic and lithologic control on catchment-wide denudation rates derived from cosmogenic ^{10}Be in two mountain ranges at the margin of NE Tibet, *Geomorphology*, *117*(1–2), 130–142, doi:10.1016/j.geomorph.2009.11.019.

Passalacqua, P., T. Do Trung, E. Foufoula-Georgiou, G. Sapiro, and W. E. Dietrich (2010), A geometric framework for channel network extraction from lidar: Nonlinear diffusion and geodesic paths, *J. Geophys. Res.*, *115*, F01002, doi:10.1029/2009JF001254.

Pelletier, P. D., and M. L. Cline (2007), Nonlinear slope-dependent sediment transport in cinder cone evolution, *Geology*, *35*(12), 1067–1070, doi:10.1130/G23992A.1.

Porder, S., P. M. Vitousek, O. A. Chadwick, C. P. Chamberlain, and G. E. Hilley (2007), Uplift, erosion, and phosphorus limitation in terrestrial ecosystems, *Ecosystems*, *10*(1), 159–171, doi:10.1007/s10021-006-9011-x.

Riebe, C. S., J. W. Kirchner, D. E. Granger, and R. C. Finkel (2000), Erosional equilibrium and disequilibrium in the Sierra Nevada, inferred from cosmogenic ^{26}Al and ^{10}Be in alluvial sediment, *Geology*, *28*(9), 803–806, doi:10.1130/0091-7613(2000)28<803:EEADIT>2.0.CO;2.

Riebe, C. S., J. W. Kirchner, D. E. Granger, and R. C. Finkel (2001a), Strong tectonic and weak climatic control of long-term chemical weathering rates, *Geology*, *29*(6), 511–514, doi:10.1130/0091-7613(2001)029<0511:STAWCC>2.0.CO;2.

Riebe, C. S., J. W. Kirchner, D. E. Granger, and R. C. Finkel (2001b), Minimal climatic control on erosion rates in the Sierra Nevada, California, *Geology*, *29*(5), 447–450, doi:10.1130/0091-7613(2001)029<0447:MCCOER>2.0.CO;2.

Riggins, S. G., R. S. Anderson, S. P. Anderson, and A. M. Tye (2011), Solving a conundrum of a steady-state hilltop with variable soil depths and production rates, Bodmin Moor, UK, *Geomorphology*, *128*(1–2), 73–84, doi:10.1016/j.geomorph.2010.12.023.

Roering, J. J. (2008), How well can hillslope evolution models "explain" topography? Simulating soil transport and production with high-resolution topographic data, *Geol. Soc. Am. Bull.*, *120*(9–10), 1248–1262, doi:10.1130/B26283.1.

Roering, J. J., J. W. Kirchner, and W. E. Dietrich (1999), Evidence for nonlinear, diffusive sediment transport on hillslopes and implications for landscape morphology, *Water Resour. Res.*, *35*(3), 853–870, doi:10.1029/1998WR900090.

Roering, J. J., J. W. Kirchner, L. S. Sklar, and W. E. Dietrich (2001a), Hillslope evolution by nonlinear creep and landsliding: An experimental study, *Geology*, *29*(2), 143–146, doi:10.1130/0091-7613(2001)029<0143:HEBNCA>2.0.CO;2.

Roering, J. J., J. W. Kirchner, and W. E. Dietrich (2001b), Hillslope evolution by nonlinear, slope-dependent transport: Steady state morphology and equilibrium adjustment timescales, *J. Geophys. Res.*, *106*(B8), 16,499–16,513, doi:10.1029/2001JB000323.

Roering, J. J., J. T. Perron, and J. W. Kirchner (2007), Functional relationships between denudation and hillslope form and relief, *Earth Planet. Sci. Lett.*, *264*(1–2), 245–258, doi:10.1016/j.epsl.2007.09.035.

Roering, J. J., J. Marshall, A. M. Booth, M. Mort, and Q. S. Jin (2010), Evidence for biotic controls on topography and soil production, *Earth Planet. Sci. Lett.*, *298*(1–2), 183–190, doi:10.1016/j.epsl.2010.07.040.

Saleeby, J., and Z. Foster (2004), Topographic response to mantle lithosphere removal in the southern Sierra Nevada region, *Calif. Geol.*, *32*(3), 245–248, doi:10.1130/G19958.1.

Saleeby, J., Z. Saleeby, E. Nadin, and G. Maheo (2009), Step-over in the structure controlling the regional west tilt of the Sierra Nevada microplate: Eastern escarpment system to Kern Canyon system, *Int. Geol. Rev.*, *51*(7–8), 634–669, doi:10.1080/00206810902867773.

Schmidt, J., I. S. Evans, and J. Brinkmann (2003), Comparison of polynomial models for land surface curvature calculation, *Int. J. Geogr. Inf. Sci.*, *17*(8), 797–814, doi:10.1080/1365881031000596058.

Schmidt, K. M., and D. R. Montgomery (1995), Limits to relief, *Science*, *270*(5236), 617–620, doi:10.1126/science.270.5236.617.

Sklar, L., and W. E. Dietrich (1998), River longitudinal profiles and bedrock incision models: Stream power and the influence of sediment supply, in *Rivers Over Rock: Fluvial Processes in Bedrock Channels*, *Geophys. Monogr. Ser.*, vol. 107, edited by K. J. Tinkler and E. E. Wohl, pp. 237–260, doi:10.1029/GM107p0237, AGU, Washington, D. C.

Small, E. E., and R. S. Anderson (1995), Geomorphically driven late Cenozoic rock uplift in the Sierra Nevada, California, *Science*, *270*(5234), 277–281, doi:10.1126/science.270.5234.277.

Small, E. E., R. S. Anderson, J. L. Repka, and R. Finkel (1997), Erosion rates of alpine bedrock summit surfaces deduced from in situ ^{10}Be and ^{26}Al, *Earth Planet. Sci. Lett.*, *150*(3–4), 413–425, doi:10.1016/S0012-821X(97)00092-7.

Snyder, N. P., K. X. Whipple, G. E. Tucker, and D. J. Merritts (2000), Landscape response to tectonic forcing: Digital elevation model analysis of stream profiles in the Mendocino triple junction region, northern California, *Geol. Soc. Am. Bull.*, *112*(8), 1250–1263, doi:10.1130/0016-7606(2000)112<1250:LRTTFD>2.0.CO;2.

Snyder, N. P., K. X. Whipple, G. E. Tucker, and D. J. Merritts (2003a), Channel response to tectonic forcing: Field analysis of stream morphology and hydrology in the Mendocino triple junction region, northern California, *Geomorphology*, *53*, 97–127, doi:10.1016/S0169-555X(02)00349-5.

Snyder, N. P., K. X. Whipple, G. E. Tucker, and D. J. Merritts (2003b), Importance of a stochastic distribution of floods and erosion thresholds in the bedrock river incision problem, *J. Geophys. Res.*, *108*(B2), 2117, doi:10.1029/2001JB001655.

Stock, G. M., R. S. Anderson, and R. C. Finkel (2004), Pace of landscape evolution in the Sierra Nevada, California, revealed by cosmogenic dating of cave sediments, *Geology*, *32*(3), 193–196, doi:10.1130/G20197.1.

Stock, G. M., R. S. Anderson, and R. C. Finkel (2005), Rates of erosion and topographic evolution of the Sierra Nevada, California, inferred from cosmogenic ^{26}Al and ^{10}Be concentrations, *Earth Surf. Processes Landforms*, *30*(8), 985–1006, doi:10.1002/esp.1258.

Stock, J. D., and W. E. Dietrich (2006), Erosion of steepland valleys by debris flows, *Geol. Soc. Am. Bull.*, *118*(9–10), 1125–1148, doi:10.1130/B25902.1.

Stock, J. D., D. R. Montgomery, B. D. Collins, W. E. Dietrich, and L. Sklar (2005), Field measurements of incision rates following bedrock exposure: Implications for process controls on the long profiles of valleys cut by rivers and debris flows, *Geol. Soc. Am. Bull.*, *117*(1–2), 174–194, doi:10.1130/B25560.1.

Stone, J. O. (2000), Air pressure and cosmogenic isotope production, *J. Geophys. Res.*, *105*(B10), 23,753–23,759, doi:10.1029/2000JB900181.

Strahler, A. N. (1950), Equilibrium theory of erosional slopes approached by frequency distribution analysis, Part II, *Am. J. Sci.*, *248*, 800–814, doi:10.2475/ajs.248.11.800.

Strahler, A. N. (1952), Hypsometric (area-altitude) analysis of erosional topography, *Geol. Soc. Am. Bull.*, *63*(11), 1117–1142, doi:10.1130/0016-7606(1952)63[1117:HAAOET]2.0.CO;2.

Tucker, G. E., and D. N. Bradley (2010), Trouble with diffusion: Reassessing hillslope erosion laws with a particle-based model, *J. Geophys. Res.*, *115*, F00A10, doi:10.1029/2009JF001264.

Tucker, G. E., and G. R. Hancock (2010), Modelling landscape evolution, *Earth Surf. Processes Landforms*, *35*, 28–50, doi:10.1002/esp.1952.

Tucker, G. E., S. W. McCoy, A. C. Whittaker, G. P. Roberts, S. T. Lancaster, and R. Phillips (2011), Geomorphic significance of postglacial bedrock scarps on normal-fault footwalls, *J. Geophys. Res.*, *116*, F01022, doi:10.1029/2010JF001861.

Unruh, J. R. (1991), The uplift of the Sierra Nevada and implications for late Cenozoic epeirogeny in the western Cordillera, *Geol. Soc. Am. Bull.*, *103*(11), 1395–1404, doi:10.1130/0016-7606(1991)103<1395:TUOTSN>2.3.CO;2.

Wakabayashi, J., and T. L. Sawyer (2001), Stream incision, tectonics, uplift, and evolution of topography of the Sierra Nevada, California, *J. Geol.*, *109*(5), 539–562, doi:10.1086/321962.

Warhaftig, C., and J. H. Birman (1965), The Quaternary of the Pacific mountain system, in *The Quaternary of the United States*, edited by H. E. J. Wright and D. G. Frey, pp. 299–340, Princeton Univ. Press, Princeton, N. J.

Whipple, K. X. (2001), Fluvial landscape response time: How plausible is steady-state denudation?, *Am. J. Sci.*, *301*(4–5), 313–325, doi:10.2475/ajs.301.4-5.313.

Whipple, K. X., and G. E. Tucker (1999), Dynamics of the stream-power river incision model: Implications for height limits of mountain ranges, landscape response timescales, and research needs, *J. Geophys. Res.*, *104*(8), 17,661–17,674, doi:10.1029/1999JB900120.

Whittaker, A. C., P. A. Cowie, M. Attal, G. E. Tucker, and G. P. Roberts (2007a), Bedrock channel adjustment to tectonic forcing: Implications for predicting river incision rates, *Geology*, *35*(2), 103–106, doi:10.1130/G23106A.1.

Whittaker, A. C., P. A. Cowie, M. Attal, G. E. Tucker, and G. P. Roberts (2007b), Contrasting transient and steady-state rivers crossing active normal faults: New field observations from the Central Apennines, Italy, *Basin Res.*, *19*, 529–556, doi:10.1111/j.1365-2117.2007.00337.x.

Wilkinson, M. T., J. Chappell, G. S. Humphreys, K. Fifield, B. Smith, and P. Hesse (2005), Soil production in heath and forest, Blue Mountains, Australia: Influence of lithology and palaeoclimate, *Earth Surf. Processes Landforms*, *30*(13), 1683–1685, doi:10.1002/esp.1311.

Wobus, C., K. X. Whipple, E. Kirby, N. Snyder, J. Johnson, K. Spyropolou, B. Crosby, and D. Sheehan (2006a), Tectonics from topography: Procedures, promise, and pitfalls, *Spec. Pap. Geol. Soc. Am.*, *398*, 55–74, doi:10.1130/2006.2398(04).

Wobus, C. W., B. T. Crosby, and K. X. Whipple (2006b), Hanging valleys in fluvial systems: Controls on occurrence and implications for landscape evolution, *J. Geophys. Res.*, *111*, F02017, doi:10.1029/2005JF000406.

Yoo, K., and S. M. Mudd (2008a), Discrepancy between mineral residence time and soil age: Implications for the interpretation of chemical weathering rates, *Geology*, *36*(1), 35–38, doi:10.1130/G24285A.1.

Yoo, K., and S. M. Mudd (2008b), Toward process-based modeling of geochemical soil formation across diverse landforms: A new mathematical framework, *Geoderma*, *146*(1–2), 248–260, doi:10.1016/j.geoderma.2008.05.029.

Yoo, K., B. Weinman, S. M. Mudd, M. Hurst, M. Attal, and K. Maher (2011), Evolution of hillslope soils: The geomorphic theater and the geochemical play, *Appl. Geochem.*, *26*, S149–S153, doi:10.1016/j.apgeochem.2011.03.054.

Zevenbergen, L. W., and C. R. Thorne (1987), Quantitative analysis of land surface topography, *Earth Surf. Processes Landforms*, *12*(1), 47–56, doi:10.1002/esp.3290120107.

M. Attal, M. D. Hurst, S. M. Mudd, and R. Walcott, School of Geosciences, University of Edinburgh, Drummond Street, Edinburgh EH8 9XP, UK. (m.d.hurst@sms.ed.ac.uk)

K. Yoo, Department of Soil, Water, and Climate, University of Minnesota, 439 Borlaug Hall, 1991 Upper Buford Cir., St. Paul, MN 55108-6028, USA.